Journal of African Earth Sciences 198 (2023) 104793

Contents lists available at ScienceDirect

Journal of African Earth Sciences

journal homepage: www.elsevier.com/locate/jafrearsci

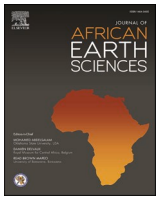

Litho-structural mapping and structural evolution of the Bocaranga pluton, northwest Adamawa-Yadé domain, Central African Republic

Rodrigue Martial Topien [a,*], Gaetan Moloto-A-Kenguemba [a], Mamadou Traore [b], Sankaran Rajendran [c], Brice Roland Kouassi [d]

[a] Geosciences Laboratory, Department of Geology, Faculty of Sciences, University of Bangui, Central African Republic
[b] Afrigeo Research Center and Engineering Firm, Bangui, Central African Republic
[c] Environmental Science Center, Qatar University, P.O. Box: 2713, Doha, Qatar
[d] UFR Sciences Biologiques, Département Géosciences, Université Peleforo Goncoulibaly, Cote d'Ivoire

ARTICLE INFO

Keywords:
Landsat mapping
Petrography
Ductile shear zone
Pan-African
Bocaranga pluton
Adamawa-Yadé
Central African Republic

ABSTRACT

The Bocaranga pluton, in the northern domain of the Central African Orogenic Belt (CAOB) in the Central African Republic (CAR), is located in the Adamawa-Yadé domain, near the Mbéré Shear Zone (MBSZ). This study provides new results of the satellite image processing, the detailed structural and petrographic studies of Bocaranga pluton which helps to understand the emplacement mechanism of this pluton. Image processing of the satellite data and field showed the occurrence and spatial distribution of (1) amphibole-pyroxenites, (2) garnet-biotite rich amphibolite, (3) migmatite, (4) hornblende-biotite and hornblende-garnet gneiss, (5) hornblende-biotite granite (HBG), (6) two micas granite (TMG), (7) fine-grained biotite granite (FBG), and (8) coarse-grained biotite granite (CBG) rock types. The mapping of regional lineaments was carried out by automatic and manual lineament extraction methods. NE-SW direction corresponds to the direction of S2 and S3 foliations, faults, mineral lineation, quartz vein, dyke (aplitic granitic or pegmatitic). NW-SE direction also corresponds to the direction of S1 foliation, F1 folds, faults, quartz veins, dykes (aplitic granitic or pegmatitic). In the absence of absolute geochronological data in study area, it has been possible to propose a polyphase structural evolution, deduced from the relative chronology of the Bocaranga granitoid. Three phases of deformation can be defined in this study. D1 phase is represented by early NW-SE trending foliation (S1) that has been progressively rotated parallel to S2 overprinting foliation occurring in gneiss, amphibolites and hornblende-biotite granite (HBG) intrusion as well. D2 phase of ductile sinistral sense from NE-SW to ENE-WSW is responsible for an emplacement of Bocaranga granitic pluton. The scarcity of structure orientation in the TMG and FBG (except the contact zones), would imply that these granites would have been crystallized in the absence of any stress. D3 is a phase of brittle deformation with three main directions corresponding to the main direction of the shear zones in the Northern domain of the CAR Pan-African fold belt.

The mylonitic deformation observed in study area illustrates the intensity of the deformation. The dominance of ellipsoidal structures observed in Bocaranga area suggests that the shear mechanism is the main controlling structure of Bocaranga granite emplacement, which can be correlated with the emplacement of Tamkoro-Bossangoa granitoid in CAR and the Adamawa-Yadé domain in Cameroon, Chad and NE Brazil.

These results imply a syntectonic emplacement of Bocaranga pluton during sinistral simple shear regime related to deformation along the Central Cameroon Shear Zone (CCSZ).

1. Introduction

In the geological reconstruction of NE Brazil and central Africa at the end of the Neoproterozoic, Bozoum-Ndélé Shear Zone (BOSZ) appears as the prolongation of the major Brasiliano shear zones of the Borborema Province of NE Brazil (Fig. 1a), either for Patos shear zone or for Pernambuco shear zone (Caby et al., 1991; Vauchez et al., 1995; Brito Neves et al., 2002; Cordani et al., 2003; Fossen et al., 2022). The BOSZ is a major lineament of Central African Pan-African Orogen. The general tectonic significance of Pan-African structures in the northwestern part

* Corresponding author.
E-mail address: topienrodriguemartial@gmail.com (R.M. Topien).

https://doi.org/10.1016/j.jafrearsci.2022.104793
Received 13 January 2022; Received in revised form 11 November 2022; Accepted 15 November 2022
Available online 22 November 2022

of the Central African Republic is poorly understood. Bocaranga pluton belongs to the so-called syn– to late–tectonic intrusions of the Central African fold belt (CAFB), in Central African Republic (CAR). This belt includes two lithostructural domains (Fig. 1a): the northern and southern domains. The northern domain is located between Mbéré Shear Zone (MBSZ) in the north and Bozoum-Ndélé shear zone (BOSZ) in the south (Mapoka et al., 2011; Topien, 2012, Fig. 1a). This domain consists of 1.8 Ga dated meta-sediments and orthogneiss (Lavreau and Poidevin, 1990) intruded by syn-to late-tectonic granitoid dated 595 to 630 Ma (Rolin, 1995; Danguene et al., 2014). The available petrographic, structural and geochemical data on a few granitoids (Mapoka et al., 2011; Topien, 2012; Danguene et al., 2014) are compatible with the subduction to post-collisional tectonic settings. These granitoids are calc-alkaline and mostly metaluminous rather than (slightly) peraluminous (Topien, 2012; Danguene et al., 2014). They were successively emplaced during the subduction up to the post-collisional stages of the Pan–African tectonic evolution.

The southern domain is divided into two units: (i) the southern unit that represents the northern part of the Congo Craton and (ii) the intermediate unit that consists of Archean gneisses, metabasites, granites and Paleoproterozoic metasedimentary rocks and migmatites. According to Rolin (1992) these rocks are separated from the Neoproterozoic gneisses by a ductile shear zone.

In the Northwestern part of the CAR, geological studies based on petrography, structural analysis, geochemistry and geochronology are poorly known in Bocoranga area.

The present work is focussed on detailed petrography an structural analysis using remote sensing and field data. These methods will allow us to constrain the tectonic evolution and emplacement mechanism of different lithological units of the Bocaranga area.

2. Geology of Bocaranga region

Bocaranga area is located in the northern domain of Pan-African Orogen formations of the Neoproterozoic age that occurred in the CAFB (Fig. 1a; Bessoles and Trompette, 1980), also known as Pan-African North Equatorial Fold Belt (Nzenti et al., 1988) linked to the Trans-Saharan Belt of western Africa and the Brasiliano Orogen of NE Brazil. Jackson and Ramsay (1980) stated that the CAFB was remobilized between 700 and 500 Ma and is located between the Congo craton and the Sahara metacraton. The belt is divided into two main domains: southern and northern (also called Yadé or Adamawa-Yadé (Penaye et al., 2004; Njiosseu et al., 2005; Toteu et al., 2006; Tchameni et al., 2006; Tcheumenak et al., 2014; Ganwa et al., 2016; Gutierrez-Aguilar et al., 2021; Toteu et al., 2022); Fig. 1a) domains.

2.1. The southern domain

The southern domain of the CAFB in CAR that extends from the Congo craton to Adamawa-Yadé domain (Pin and Poidevin, 1987; Poidevin, 1991) is divided into two units:

- (i) the southern unit, that registred 3432 Ma (Rb/Sr on total rocks) and 3417 ± 14 Ma (Pb-Pb model age) according to Poidevin et al. (1981); Poidevin (1991)), representing the northern border of the Congo Craton. It is made of protoliths of tholeitic basalts and gabbros of mafic and ultramafic rocks of Mbomou corresponding to a suite of affinity depleted oceanic basalts and gabbros (N-MORB) associated to rare iron-bearing sediments on one hand and trondhjemitic gneisses of Nzangi on the other hand. The Mbomou amphibolo-pyroxenite complex is considered by Poidevin (1991) as part of "obducted" oceanic crust dated between 3.7 and 3.4 Ga.
- (ii) the intermediate unit is made of a lower unit composed of quartzite, garnet micaschists, orthogneiss and amphibolite and an

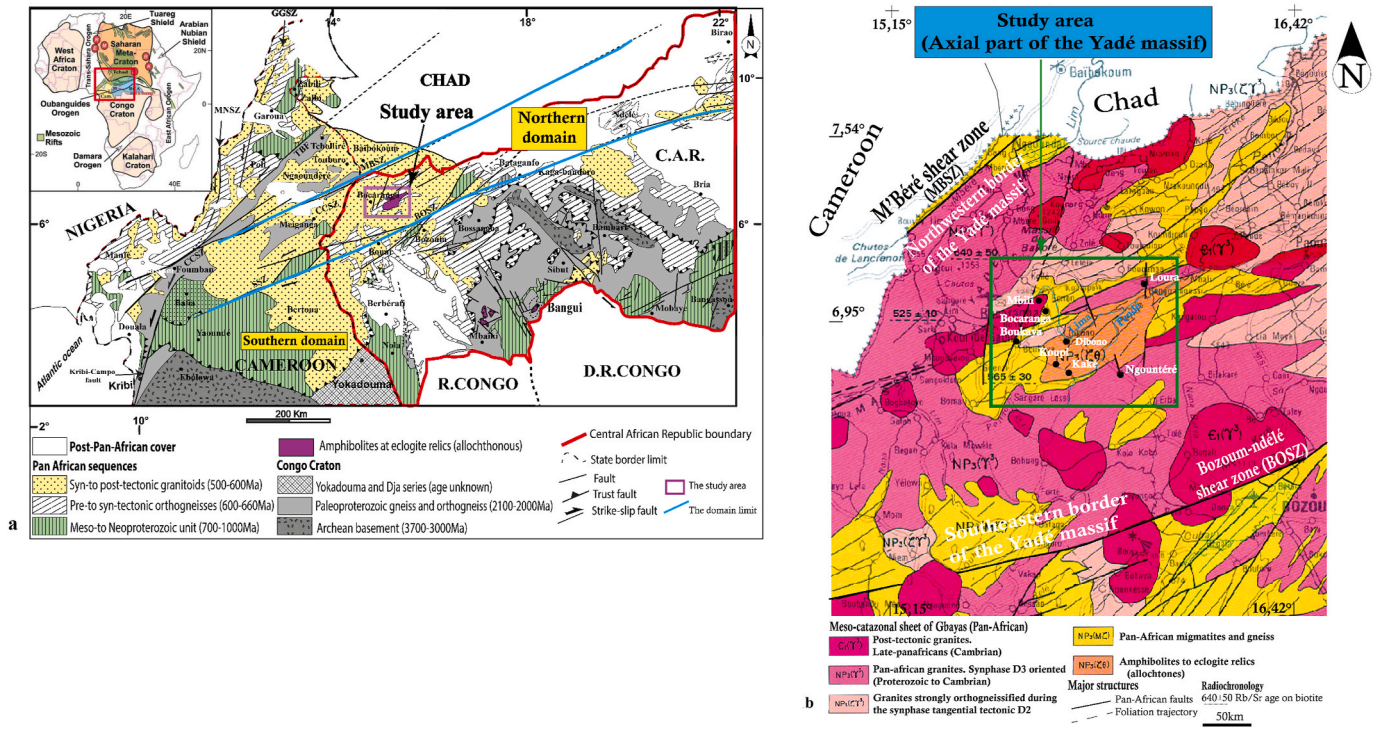

Fig. 1. a). Geological map of Central Africa (after Poidevin, 1991; Rolin, 1995; Toteu et al., 2001; Toteu et al., 2004; Toteu et al., 2006; Ngako et al., 2003; Njonfang et al., 2006; Tchakounté et al., 2017) showing the main litho-tectonic units and domains of the Central-African Orogenic Belt (SZ - Shear Zone; CCSZ - Central Cameroon shear zone; MNSZ - Mayo Nolti shear zone; SSZ - Sanaga shear zone; MBSZ- M'Béré shear zone; BOSZ - Bozoum-Ndélé shear zone; TBF - Tcholliré Banyo Fault; CAR - Central African Republic; R.Congo -Congo Republic; D.R. Congo - Democratic Republic of Congo and **b).** Petro-structural map of northwestern CAR (after Rolin, 1995).

upper unit composed of quartzite and chloritoschist. Both units are both intruded by Eburnean granitoids dated at 2.1 Ga (U-Pb age on zircon; Poidevin and Pin, 1983). Lavreau et al. (1990) suggested a monocyclic evolution for this intermediate unit.

2.2. The northern domain

The CAR northern domain corresponds to the Central domain of the Central Africa Panafrican belt in Cameroon and Chad (Cornacchia and Dars, 1983; Toteu et al., 2001, 2004; Kwékam et al., 2010 Mapoka et al., 2011; Topien, 2012; Danguene et al., 2014; Saha-Fouotsa et al., 2021; Seguem et al., 2022). Fig. 1b shows the different lithological units and structures that occur in the NE-SW direction parallel to the brittle structures in the geological map of Bocaranga area (Rolin, 1995). The map shows the occurrence of amphibolite units in the Bocaranga area with eclogite relics.

Yadé massif, also known as Mbaïbokoum massif (Seguem and Klötzli, 2014; Seguem et al., 2022), is bounded by the Bozoum-Ndélé shear zone in the south (Cornacchia and Dars, 1983; Dumont, 1986; Lavreau and Poidevin, 1990; Rolin, 1995). The latter is an eastward extension of the Sanaga shear zone located in Cameroon (Ngako et al., 1991, 2003, 2008). The northwestern part of this massif is bounded by the M'Béré shear zone (Rolin, 1992), an eastward extension of the Central Cameroon Shear Zone (CCSZ), also called Adamawa Shear Zone (Njanko et al., 2006, Fig. 1a). Bocaranga area is located within the Yadé massif (Fig. 1b). The domain is characterized by the presence of extensive tracts of Paleoproterozoic metasedimentary rocks and orthogneisses (Toteu et al., 2004; Mapoka et al., 2011). From Sm-Nd model ages and inherited zircon ages, Toteu et al. (2004) suggested that the metasedimentary and orthogneisses of Adamawa-Yadé domain contain significant contribution of an Archean crust similar in the age to the Congo craton (Tchakounté et al., 2017). Toteu et al. (2004) also reported that these rocks preserve relics of Paleoproterozoic (~2.1 Ga) significantly obliterated by Neoproterozoic deformation.

The Adamawa-Yadé Domain is considered as an Archean domain reworked during the Paleoproterozoic (Ganwa et al., 2016; Toteu et al., 2001; Penaye et al., 2004) as a piece of the Archean Congo craton detached during 1000-700 Ma Neoproterozoic rifting that preceded the Pan-African collision during 654-600 Ma. The studied rocks have not yet been dated in the past.

3. Materials and methods

3.1. Satellite data

In this study, the petro-structural map of the CAR (1:1,500,000; Rolin, 1995), a geomorphological map of the western sheet of CAR (1:1, 000,000; Boulvert, 1995), and satellite images of Landsat-8 and Digital Elevation Model (DEM) of Shuttle Radar Topography Mission (SRTM) were used. The Landsat 8 satellite carries two sensors: the Operational Land Imager (OLI) and the Thermal Infrared Sensor (TIRS). Both instruments collect data jointly to provide coincident images of the same surface areas. The OLI acquires surface energy over a 185 km swath in nine spectral bands including a panchromatic band in the visible, near-infrared, and shortwave infrared wavelength regions using long linear detector arrays, which have thousands of detectors per spectral band. The OLI collects data with 14 bits of radiometric precision, while only transmitting 12 bits to the ground to save bandwidth. The bands have higher signal-to-noise performance and 30 m spatial resolution, except for the panchromatic band 8, which has 15 m spatial resolution in a "push-broom" manner. The widths of several OLI bands are refined to avoid atmospheric absorption features. The TIRS is also a push-broom sensor that uses long arrays of photosensitive Quantum Well Infrared Photodetectors (QWIPs) and measures longwave thermal infrared (TIR) energy emitted by the Earth's surface. The QWIPs of TIRs are sensitive and enable the separation of the temperature of the Earth's surface. The TIRs collect thermal energy in two spectral bands at 100 m spatial resolution quantized to 12 bits. The quality of data (12-bits) of the OLI and TIRs is higher than previous Landsat instruments (8-bit for TM and ETM+) which provide significant improvement in the ability to detect features of the Earth's surface.

In this study, a cloud-free Landsat 8 OLI level 1T data of 01/09/2019 and the 30 m spatial resolution DEM data of 018/09/2020 were acquired for the Bocaranga region from the USGS Data Management and Information Distribution (DMID) (https://glovis.usgs.gov/) to map the different lithological units and extract the lineaments of the region. The sensor characteristics of the Landsat-8 OLI are given in Table 1.

3.1.1. Pre-processing of Landsat-8 OLI images

The satellite data was calibrated to 5% uncertainty in terms of top of atmosphere reflectance or absolute spectral radiance. The acquisition of this data was made in the absence of clouds. They were recorded in UTM zone 33N in a WGS 84 geodetic reference system. They were applied to radiometric correction, converting digital numbers (DN) to Top of Atmosphere (TOA) Radiance. Raw luminance data from the imaging spectrometer was scaled to reflectance data using the FLAASH (Fast Line-of-sight Atmospheric Analysis of Spectral Hypercubes) algorithm by providing appropriate local values for several parameters in ENVI® (version 5.5).

The mapping of geological formations and the extraction of lineament structures of the region are carried out using the ENVI, PCI Geomatica 2017, ArcGIS 10.3, and Rockworks software. The schematic diagram (Fig. 2) shows steps of the pre-processing and the image processing of Landsat 8 OLI and DEM data.

3.2. Image processing

Lithological mapping and lineament extraction of Bocaranga region carried out using respectively (i) OLI data by developing False Color Composites (FCC), principal component analysis (PCA), and band ratio methods as described below and (ii) SRTM DEM data by applying directional filtering.

3.2.1. False color composite (FCC)

The different bands of Landsat 8 that are characteristic of spectral band absorptions of different rock types of Bocaranga region were chosen in red, green, and blue (RGB) channels and developed FCC images were used for mapping the geological formations of the study area.

Table 1
Sensor characters of Landsat 8.

Sensor Characters	Landsat 8 (OLI/TIRS)
Spectral bands (all bands in μm)	P) 0.50–0.68 VNIR 1) 0.43–0.45 Coastal 2) 0.45–0.51 VNIR 3) 0.53–0.59 VNIR 4) 0.63–0.67 VNIR 5) 0.85–0.88 NIR 6) 1.57–1.65 SWIR 1 7) 2.11–2.29 SWIR2 9) 1.36–1.38 Cirrus 10) 10.6–11.19 TIRS1 11) 11.5–12.51 TIRS2
Swath width	185 km
Spatial resolution	15 m PAN 30 m VNIR/SWIR 100m TIR
Radiometric resolution	16 bit
Band-to-band registration	0.2 pixel (90%)
Geodetic accuracy without ground control	400 m (90%)
Data rate	384 Mbps on X-band 260.92 Mbps on S-band
Instrument mass	2071 kg fully loaded
Average power	125 A-Hour

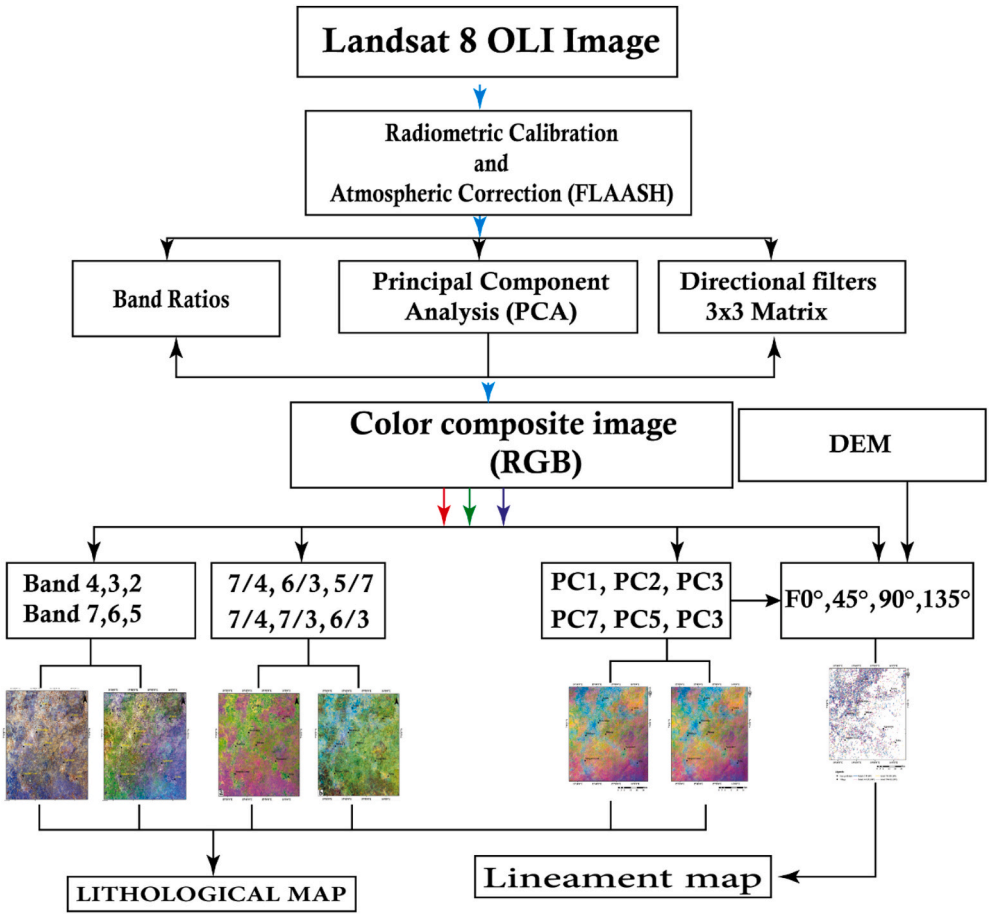

Fig. 2. The schematic diagram shows the pre-processing and image processing of the Landsat 8 data for the mapping of geology and lineament structures of the Bocaranga region.

The RGB image displays image features in a combination of three spectral bands using the three primary colors at a time as a color composite. The resulting image exhibits each pixel with a color determined by the combination of the RGB of different brightness and the image depicts features in different colors that differ from a true-color image. A statistical analysis for seven bands having the same spatial resolution (USGS, February 13, 2020) is used to develop the False Color Composites (FCC) by studying the correlation coefficient and standard deviations of bands. The highest band combination (Table 1) of the optimum index factor (OIF) was chosen as the most favorable band combination in this study.

3.2.2. *Principal component analysis (PCA)*

The Principal Component Analysis is a linear transformation technique also known as eigenvector transformation. It transforms multivariate data comprising a set of correlated variables (*i.e.* spectral channels) in an uncorrelated coordinate system (*i.e.* principal components). In this new orthogonal coordinate system, which arises from the rotation and shifting of the old one, the first component contains most of the original data variance, while succeeding components contain decreasing proportions of data variation, mainly containing unexplained residual variance. The PCA is very useful, especially in multi-temporal studies, as it eliminates differences due to different atmospheric conditions or sun angles. The variance-covariance or the correlation matrix can be derived either from the total number of pixels in the satellite image or from a subset. The PCA is used to extract and place spectral information into a smaller set of new components that are more interpretable. The technique has been applied for image enhancement, image data compression, merging of multiresolution and multispectral data, and different applications (Traore et al., 2021; Xiong and Zuo, 2020; Rajendran and Nasir, 2019; Rajendran et al., 2011).

iii. Band ratio (BR)

The band ratios are widely used in satellite data image analysis. This method suppresses the topographic variation and the image brightness difference related to grain size variation (Sultan et al., 1987). The selection of spectral bands for the different ratio images is based on the spectral signature of minerals and rocks. When rationing techniques are applied, all the reasonable groups of minerals and rocks are best discriminated again. The ratio may include short-wavelength bands (*i.e.* 3/1), the long-wavelength bands (*i.e.* 5/7), and a ratio of one band each from short and long wavelength band groups (*i.e.* 5/3) (Crippen, 1989). Different band ratios of Landsat-8 OLI for lithological mapping and mineral exploration have been used recently (Traore et al., 2020, 2022; Topak et al., 2022).

3.3. *Lineament extraction*

The automatic lineament extraction was performed over the PC1 channel, the panchromatic band (8), and SRTM-DEM images using PCI Geomatica 2017 software. The application of a 7 × 7 matrix Sobel directional filter is used in four directions: N0°E, N45°E, N90°E and N135°E. The discontinuities linked to road networks, buildings, cultivated areas, and redundancies have been removed manually during the lineament extractions of the Bocaranga region. The lineaments were extracted from the panchromatic image and the principal component (PC1) images. The lineaments extracted from SRTM-DEM and Landsat images were merged into one output. In this process, redundant or

duplicated lineaments were removed and the final lineament map output was obtained. A total of 300 lines were extracted from an area of 343.19 km^2. Further, the data from the SRTM satellite were used to generate a Digital Elevation Model (DEM) to facilitate the lineament extraction. DEM offers visual perspective capability, an emphasis on terrain features, and the application of a three-dimensional analysis system. Topographic features that represent lineaments such as linear valleys, linear stream segments and rocky boundaries, alignment of vegetation, etc., were manually extracted and digitized on screen. Such lineament extraction was carried out under six different azimuth angles 90°, 135°, 225°, 270°, 315° and 348° (*eg.* Das et al., 2018). In addition, the lineament extraction was performed at two different scales (1: 50, 000 and 1: 80,000) to map lineaments of all sizes. The lineaments extracted from each azimuthal angle were compared to other data sources such as topographic maps and high-resolution Google Earth images to eliminate non-geological lineaments. This elimination was performed over the maps extracted from the six different azimuth angles. After this removal process, the lineaments maps were stored in six separate shape files and further converted into a single shape file.

3.4. Field studies

Rock samples were collected from the most homogeneous rocks which appears fresh without evidence of alteration. Twenty-two rock samples of mafic and intermediate to felsic rocks were collected. They have been studied at different scales in the field and at the laboratory using a plane-polarized light microscope. Field photographs were taken during field trips and thin sections of samples were prepared at the University of Lorraine (Nancy, France). The measurement of structural elements recorded in the field was statistically analyzed and plotted using Stereonet of Rockware software (2017 version).

4. Results

4.1. Lithological mapping

4.1.1. FCC image interpretation

To discriminate rock types from Bocaranga region, the optimum index factor (OIF) values (Table 2) were studied for the highest band combination, and the best False Color Composites (FCCs) were developed using the bands 7, 6, 5 and 1. Fig. 3 shows the FCC images (R: 7; G: 6; B: 5 and R: 6; B: 5; 1) of the study area. The image developed using bands 7, 6, and 5 and overlayed by geological boundaries of Bocaranga region shows the felsic rock types including the gneiss and biotite gneiss in a purple mixed bright tone, and the amphibolite and amphibole pyroxenite exhibiting a mixture of blue and bright yellow (Fig. 3a). Whereas, the FCC developed using 6, 5, and 1 shows the greenish-yellow to purple, the amphibolites appear in dark purple (Fig. 3b). The structural features and igneous texture of rocks located in the southwestern part of the region are easily recognizable. However, both images do not show the different rock types of the region distinctly, which may be due to the presence of vegetation in the region. Thus, we studied the images developed using Principal Components Analysis (PCA).

Table 2
Optimum Index Factor (OIF) of the seven (7) bands.

Highest ranking in the OIF index			
Band 5	Band 6	Band 7	6096.17
Band 1	Band 5	Band 6	5954.49
Band 2	Band 5	Band 6	5851.01
Band 4	Band 5	Band 6	5770.28
Band 3	Band 5	Band 6	5753.17
Band 1	Band 6	Band 7	5717.65

4.1.2. Principal component analysis (PCA)

Table 3 provides the values of the eigenvector matrix of seven bands of Landsat 8 of PCA. It shows that the principal component 1 (PC1) is composed of negatively weighted eigenvectors in seven (7) bands, representing 98% of the total variance of the data and the other components decrease in turn. The eigenvector of band 5 of PC2 is much larger than the other values. PC3 and PC4 can show different lithologies due to the different contributions of positive and negative eigenvector weights in each band. However, PC5, PC6, and PC7 were eliminated due to minimal information and band noise. Therefore, the PC1, PC3, and PC4 were assigned to red, green, and blue channels respectively, leading to the resulting image (Fig. 4). The image shows the two micas granitoid (TMG) in light purple and mottled with blue, the fine-grained biotite granitoid appears in light blue, and the coarse-grained biotite granitoid in yellow to red and mottled with green.

iii. Band ratio

Different band ratios (Table 4), including the band ratios of Abrams et al. (1988); Sabins (1997); Gad and Kusky (2006) and Madani (2014) to clearly distinguish the geological formations in the study area. Ratios 6/7, 4/3, 5/6; 7/4, 6/3, 5/7; 7/6, 6/5, 4/2, and 7/4, 7/3, 6/3 are inspected and applied to the Landsat 8 OLI image of the study area (Fig. 5). Among these, the ratio image (R: 6/7, G: 4/3, B: 5/6) developed using the method of Abrams et al. (1988) highlighted the different rock types in different tones (Fig. 5).

The gneiss was observed in pink color and turned purple in the band ratio 6/7, 6/2, 6/5 (Fig. 6a) and 6/7, 6/2, 5/4 (Fig. 6b). This rock appears with pink color (Fig. 6). Hornblende-biotite granite (HBG) was also observed as light brown and mottled with green using the band ratio 7/6, 6/5, 4/2 (Fig. 6d). Coarse-grained biotite granite (CBG) was observed in blue color with green on the band ratio 7/6, 6/5, 4/2 (Fig. 6d), fine-grained biotite granite (FBG) appears with pink color and mottled with green on the band ratio 6/7, 6/2, 5/4 (Fig. 6a). Migmatites are light pink and speckled with purple on the 6/7, 6/5, 4/2 (Fig. 6c) ratio band and amphibolites are dark brown on the ratio band 6/7, 6/5, 4/2 image (Fig. 6c).

According to these results, it is evident that the Landsat 8 OLI band ratio image (6/7, 6/5, 4/2 and 7/6, 6/5, 4/2, Fig. 6c and d) and Principal Component Analysis (PC1, PC3, and PC4, Fig. 4) are powerful tool to distinguish subtle differences between the various rock units in the study area.

Field data are then combined with visual interpretation results of the various Landsat 8 OLI images to create a detailed lithological map of Bocaranga area from Figs. 6–20. This map shows differences in the distribution of some rock units and their contacts (differences between TMG, CBG, FBG, migmatites, amphibolites and gneiss; as well as the contacts between HBG and adjacent rocks) compared to the published geologic map by Rolin (1995) of the northwestern part of the CAR.

4.2. Lineament extraction and interpretation

Automatic lineament extraction was performed on PC1 channel panchromatic band (8) of Landsat-8 OLI and SRTM-DEM images. The lineament synthesis obtained from the panchromatic image (Fig. 7a) and the PC1 channel of the study area is given in Fig. 7b. On this latter, lineaments show NE-SW as preferential direction. The resulting map shows various directions of structures (Fig. 8a and b). In addition, the lineament density map shows the lineament frequency per unit area (Fig. 9a). The lineament map obtained after the various treatments shows approximately 1085 fractures of varying lengths from 0.40 km to 3.80 km with an average length of 0.91 km. The lineament map corresponding rose diagram is given in Fig. 8b. Table 5 shows the Sobel and gradient filter matrices.

Fig. 9a shows the statistical information obtained by automatic lineament mapping from Landsat-8 OLI and DEM images. According to the statistics, the total population is 300, and the total length of all

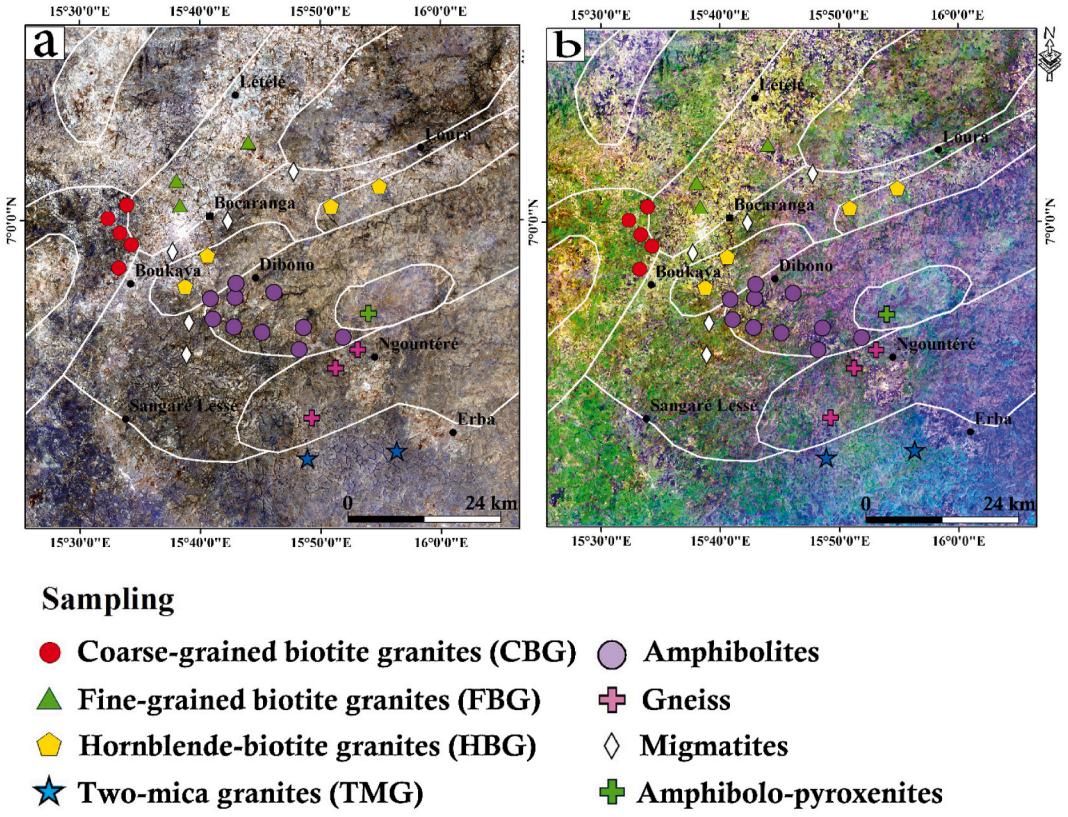

Fig. 3. False color composition in RGB of: **a)** 7, 6, 5; **b)** 6, 5, 1.

Table 3
Eigenvector matrix in seven (7) Landsat 8 OLI bands.

Principal component	Band 1	Band 2	Band 3	Band 4	Band 5	Band 6	Band 7
PC1	−0.487358	−0.466433	−0.422241	−0.429966	−0.403425	−0.133727	−0.033609
PC2	−0.318692	−0.284926	−0.099571	−0.086432	0.892079	0.060997	−0.018491
PC3	−0.404764	−0.250709	0.006479	0.756426	−0.174986	0.393555	0.124831
PC4	−0.276575	−0.047067	0.34165	0.295018	0.00585	−0.828353	−0.176997
PC5	0.288043	0.084021	−0.796646	0.376671	0.088207	−0.238755	−0.262034
PC6	0.5793	−0.791972	0.167725	0.069583	−0.016046	−0.059159	0.021458
PC7	0.045079	0.043678	−0.179599	0.041463	0.052451	−0.277197	0.939412

lineaments is 2,834,045.06 m. We observe that zones with high density lineaments are Létélé, NW Bocaranga, Sangaré Lessé, and SW of Boukaya (Fig. 9b). The discontinuities identified from the satellite bands are the basis of a frequency analysis allowing the main directions to be revealed, which can then be compared with those of the structural data recorded in the field. Global statistical analysis of Bocaranga lineaments shows two preferential directions, globally-oriented NE-SW and NW-SE (Fig. 8a–c): (i) the dominant NE-SW direction is divided into two subclasses (e.g. N030° - N040° and N060° - N070°); (ii) the less dominant NW-SE direction also includes two sub-classes (e.g. N150°- N160° and N-S).

5. Petrography and structures

In the field, it is possible to verify the results of satellite data and validate the occurrence, association, and spatial distribution of the rock types in the Bocaranga region. We are able to measure the structural elements and collect rock samples and minerals. The Bocaranga region is made of five major rock types namely (1) amphibole pyroxenites, (2) amphibolites, (3) migmatites, (4) gneiss and (5) granites (hornblende biotite granite (HBG), fine-grained biotite granite (FBG), coarse-grained biotite granite (CBG) and two mica granite (TMG). We used mineral abbreviations according to Kretz (1983).

5.1. Petrography

5.1.1. Amphibole pyroxenites

Amphibole pyroxenite, crops out in Kaké (Fig. 1b) in form of scattered boulders and SW-NE oriented slabs. Outcrops did not allow neither to observe their contact with the country-rock of gneissic nature nor with other rocks in the locality. In the field, the rock exhibits the intersected feldspathic quartz veins. It is dark greenish and massive and occurs with phenoblasts (Fig. 10a and b). The rock shows micro-grained to coronitic texture and mineral assemblages of Opx + Cpx + Pl, and Cpx + Hbl + Pl + Qtz + Op ± Ep (Fig. 10c and d). Clinopyroxenes appear as subautomorphic and xenomorphic phenoblasts. Orthopyroxene crystals are xenomorphic and show reaction rims composed of coronas Ep + Qtz + Op (Fig. 10d). Hornblende appears as subautomorphic and xenomorphic minerals of variable size. Plagioclase is in subautomorphic to xenomorphic ranges of variable size. Plagioclase is abundant and sometimes shows a destabilization into epidote. It is associated with pyroxene and hornblende.

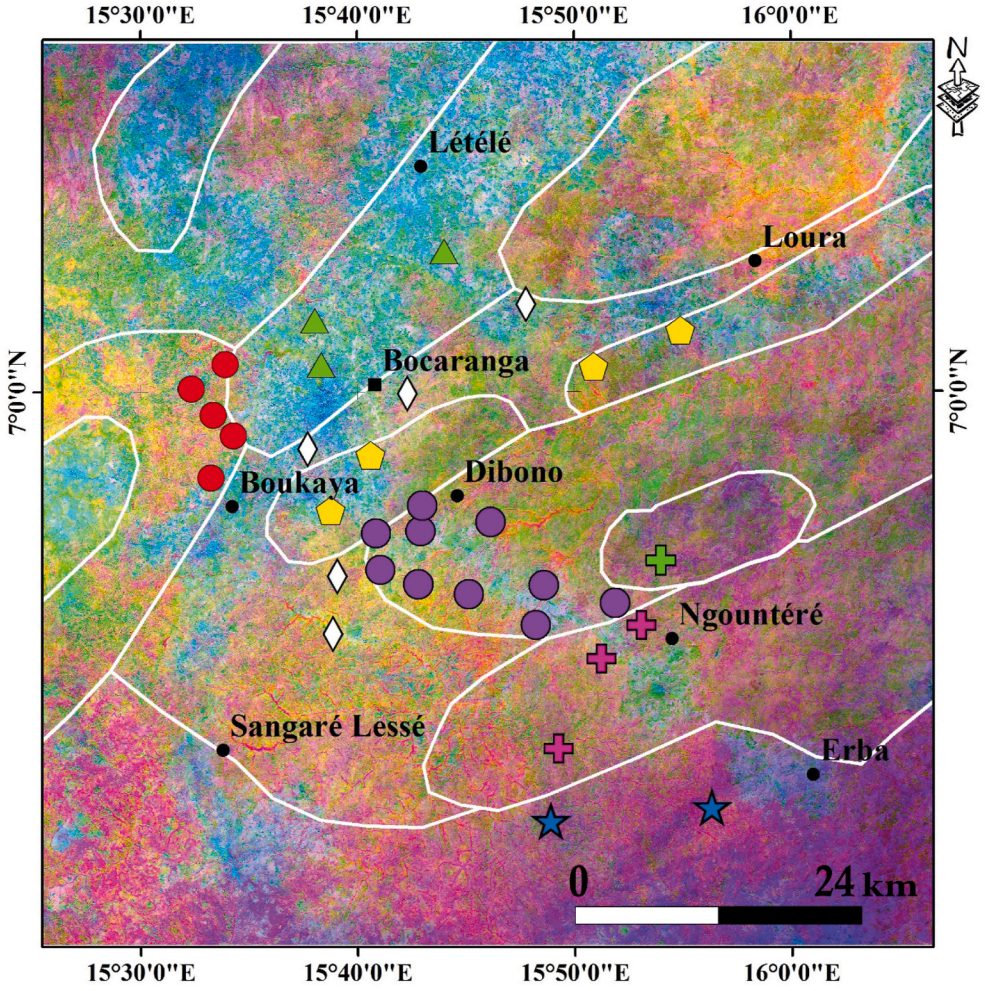

Fig. 4. RGB image of principal components PC1, PC3, PC4 shows the different lithological units of the Bocaranga region. It is the same legend as Fig. 3.

Table 4
The different band ratios used in this study.

RGB band ratio	References
6/7, 4/3, 5/6	Abrams et al. (1988)
7/4, 6/3, 5/7	Sabins (1997)
7/6, 6/5, 4/2	Gad and Kusky (2006)
7/4, 7/3, 6/3	Madani (2014)

5.1.2. Amphibolites

Three types of amphibolites are observed in the study area: a) garnet amphibolites, b) biotite amphibolites, and c) epidote amphibolites.

Garnet amphibolites crop out as slabs in Kaké locality on the banks and bed of the Pendé river. The outcrop is elongated in the NE-SW direction at the contact with garnet and amphibole gneiss (Fig. 11a). They are massive and intersected by epidote veins. The rock shows granoblastic texture (Fig. 11b) and are composed of abundant hornblende, plagioclase and garnet, and epidote, chlorite, quartz and opaque mineral (ilmenite). Hornblende and plagioclase crystals are of two generations. The first generation (Hbl1) is subautomorphic phenoblasts joined with plagioclase in the matrix while the second generation (Hbl2) is xenomorphic in form of aggregates (symplectite) around crystals. Some sections of hornblende crystals show transformations into oxide. The first generation of plagioclase shows sub-automorphic crystals while the second generation moulds some garnets porphyroblasts, in association with symplectic hornblende crystals. Garnet crystals are abundant and exhibit automorphic to subautomorphic to automorphic phenoblasts with inclusions of quartz and ilmenite (Fig. 11b). Textural relationships suggest the existence of three mineral parageneses viz. (1) Hbl1+Pl1+Grt + Qtz; (2) Hbl1+Pl1+Bt + Qtz + Ilm; and (3) Hbl2+Pl2+Qtz + Chl + Ep + Ilm; suggesting, according to Gutiérrez-Aguilar et al., (2021), that the rock presents a retrogarde mineral assemblage.

Biotite amphibolites crop out as slabs, blocks or as elongated enclaves in granites and orthogneisses. The rock display medium-to fine-grained structure with mineral preferred orientation. Sometimes, they exhibit mylonitic texture (from Dibono). The rock displays a grano-nemato-lepidoblastic texture. It is composed of hornblende xenomorphic crystals, plagioclase and biotite flaks. Hornblende is the main mineral. Their crystals show fractures, filled with epidote in association with biotite, ilmenite, titanite, and apatite (Fig. 12b). Biotite flakes, generally chloritized, have diffuse borders due to the destabilization of hornblende. Plagioclase is subautomorphic to xenomorphic. Crystals such as plagioclase are generally observed as inclusions in hornblende crystals and exhibit rounded shapes (Fig. 12b). The mineral assemblage identified is Hbl + Pl + Bt + Qtz + Ttn + Ilm; suggesting, according to Gutiérrez-Aguilar et al., (2021), that the rock presents a retrogarde mineral assemblage.

Epidote amphibolites crop out as metric to centimetric slabs at the Koupi and Boléré. They are dark green, massive, and intersected by epidote veins (Fig. 12c). The rock is rich in epidote and poor in biotite. It exhibits granular nematoblastic texture (Fig. 12d). Some hornblende

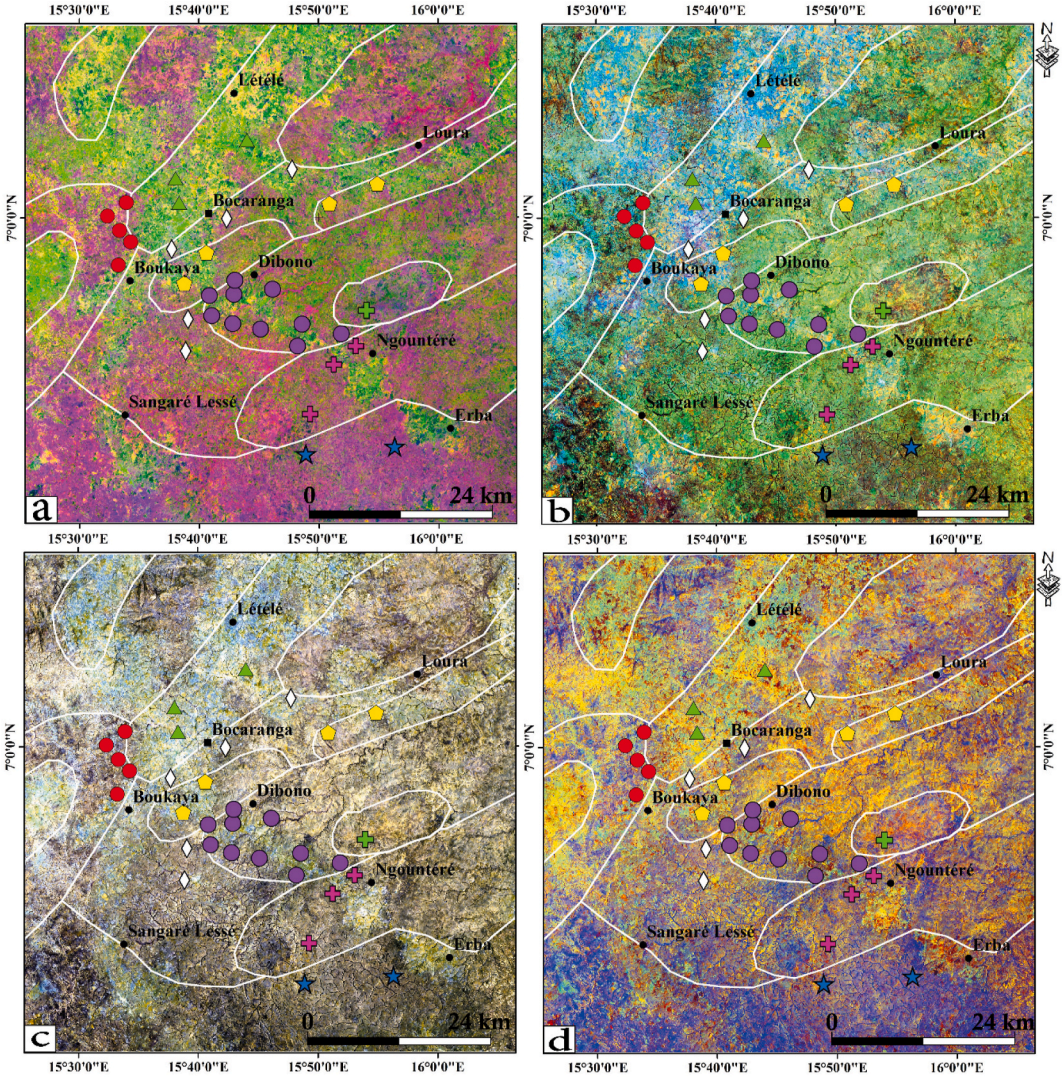

Fig. 5. a) RGB colour compositie of band ratios 6/7, 4/3, 5/6 (Abrams et al., 1988) show the different rock types of the Bocaranga region; **b)** RGB colour compositions of band ratios (7/6, 6/5, 4/2; Gad and Kusky, 2006); **c)** RGB colour compositions of band ratios (7/4, 7/3, 6/3, Madani, 2014); **d)** RGB colour compositions of band ratios (7/4, 6/3, 5/7, Sabins, 1997). It is the same legend as Fig. 3.

crystals show destabilization into chlorite, ilmenite, and epidote. Plagioclase occurs as automorphic to subautomorphic crystals which coexist with hornblende crystals. Epidote is generally associated with amphiboles and ilmenite. Quartz is xenomorphic and sometimes occurs as recrystallization micrograins around feldspar and amphibole phenoblasts. Amphibole crystals are destabilized on the rim into titanite, ilmenite, quartz and epidote. The mineral assemblage identified is Hbl + Pl + Chl + Ep + Qtz + Ttn + Ilm.

iii. Migmatites

Migmatites occur in Bocaranga region at Koumkoum, Béféré, Colbaya, Nganza, Kparkanda, Erémandji, Kpaïkanya, Haoussa and Ndouikaré. The rock is made of melanosome and leucosome (Fig. 13c). Melanosome is defined as a migmatite that preserves partially melted structures and exhibits stratification, foliation, or stratification where the melt fraction was low (Brown, 1973; Sawyer, 2008). Bocaranga migmatites are mainly stromatic consisting of numerous thin (commonly 2 mm to 5 cm) and laterally persistent bands of light colored quartzo-feldspatic leucosomes usually bounded by dark biotite-rich melanosomes (e.g. Fig. 13c). Stromatic metatexites constitute the most abundant morphologic variety among migmatites in the study area. Most leucosomes are laterally continuous and parallel to the main foliation and compositional layering but some are located at dilatant sites such as interboudin partitions and small shear bands outlining net-like patterns and cross-cutting the main foliation may be alternatively distributed as irregular patches or lenses. Many of these field relationships are shown in Fig. 13c.

5.1.4. Gneiss

Two types of gneiss are observed in the study area: hornblende garnet gneiss (HG-gneiss), and hornblende biotite gneiss (HB-gneiss).

Hornblende garnet gneiss crops out in Pendé river. The rock is elongated in NE-SW direction and presents contact with garnet amphibolite (Fig. 12a). The rocks is made up of abundant hornblende crystals, garnet, plagioclase and minor amounts of epidote, chlorite, quartz and ilmenite minerals showing preferred orientation with heterogranular grano-nematoblastic texture (Fig. 14a). Hornblende crystals, of two generations and variable size, occur as (i) subautomorphic phenoblasts in the matrix (Fig. 14a) and (ii) xenomorphic crystals in aggregate around garnet crystals. It also presents quartz and ilmenite inclusions. Garnet crystals, subautomorphic to xenomorphic, show some blasts surrounded by hornblende, plagioclase, and ilmenite. Plagioclase crystals are subautomorphic to xenomorphic crystals. Some crystals, associated to hornblende, sometimes mould garnet crystals. Biotite

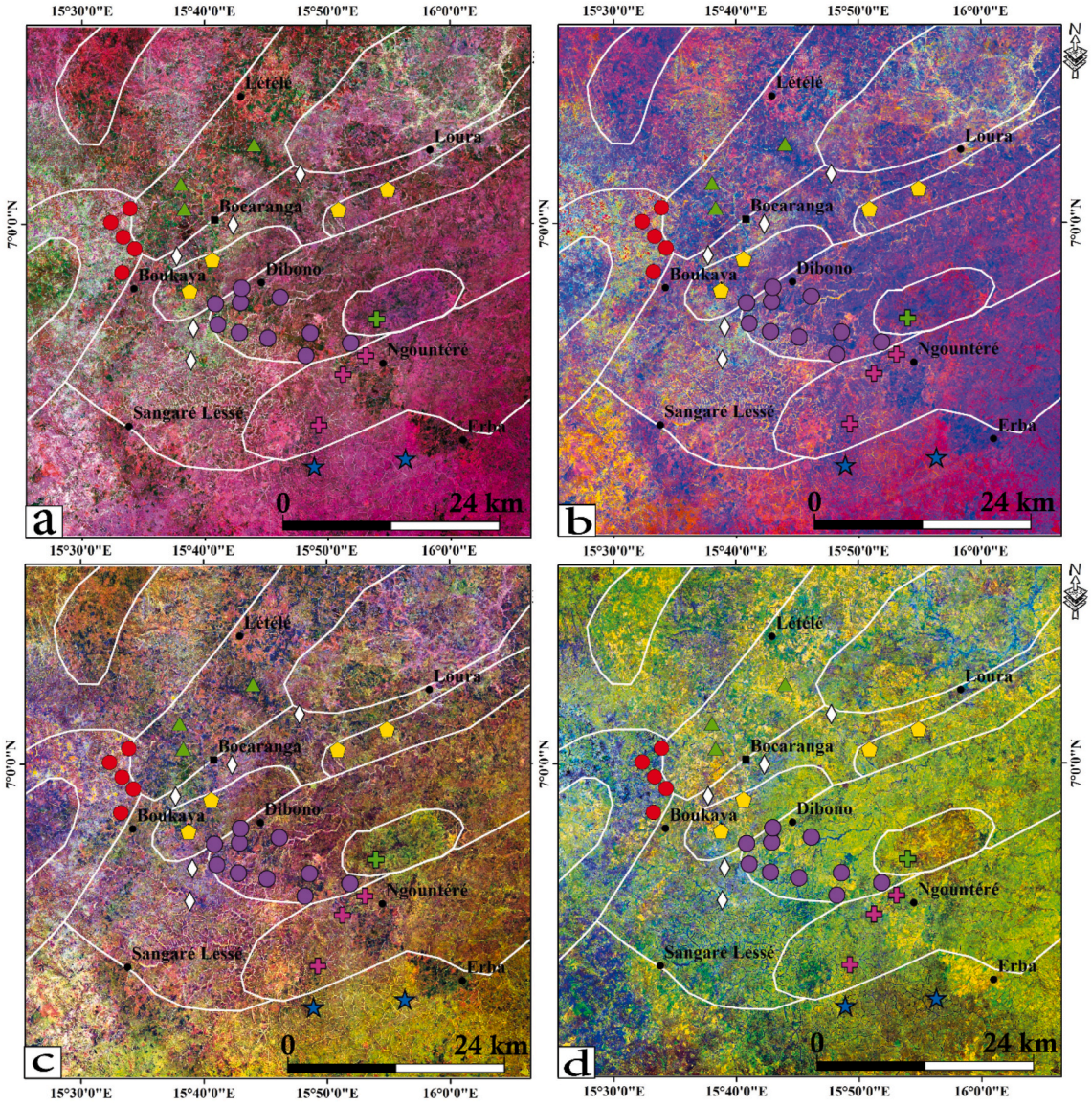

Fig. 6. RGB colour compositions of different band ratios made on Landsat 8 OLI image extracts of the Bocaranga region, northwestern CAR. **a)** Band ratio 6/7, 6/2, 6/5; **b)** Band ratio 6/7,6/2,5/4; **c)** Band ratio 6/7, 6/5, 4/2 and **d)** Band ratio 7/6, 6/5, 4/2. It is the same legend as Fig. 3.

flakes are strongly pleochroic. Quartz is xenomorphic and occurs sometimes either as elongated polycrystalline ribbons or as recrystallized micrograins around feldspar and hornblende phenoblasts. Chlorite flakes would originate from the alteration of garnet, amphibole, and biotite. Epidote crystals occur on hornblende crystals or form halos around ilmenite crystals. The mineralogical assemblages of hornblende-garnet gneiss are: (1) Hbl1+Pl1+ Qtz + Grt (2) Hbl2+Pl2+Bt + Qtz + Chl + Ep + Ilm.

Hornblende biotite gneiss (HB-gneiss) crop out as (i) NE-SW oriented slabs on the river banks (Lima (Fig. 12a) and Ngountere) and (ii) enclaves in the coarse-grained biotite granite, hornblende biotite granite and two mica granite). The rock is dark grey in color, fine-grained, and has a gneissic texture marked by alternated amphibole-rich dark and quartzo-feldpathic light bands. The rock has a granoblastic to nematoblastic texture (Fig. 14b) and is composed of quartz, feldspar, hornblende, biotite, and accessory minerals. Large sections of plagioclase often have many inclusions (biotite, amphibole), thus developing a poecilitic microtexture. K-feldspar presents perthitic exsolutions of albite and myrmekite on grain boundaries. Weakly deformed quartz is present as equidimensional neograins. Hornblende usually appears in subautomorphic to xenomorphic form. Sometimes associated with biotite flakes. The hornblende-biotite-plagioclase association is very characteristic in the dark bands. Biotite flakes are often associated with titanite and ilmenite. The mineralogical assemblages of HB-gneiss are 1) Hbl + Pl + Qtz+(Or/Mc)+ Bt, and 2) Hbl + Pl + Chl + Ep + Ser + Ttn.

5.1.5. Granites

There are four types of granites: 1) hornblende biotite granite (HBG); 2) coarse grained biotite granite (CBG); 3) fine grained biotite granite (FBG) and 4) two micas granite (TMG).

Hornblende biotite granite (HBG) crops out as slabs in Loura (northeast Bocaranga) and Dibono (southeast Bocaranga). It is intrusive in gneissic basement and contains amphibolitic and gneissic enclaves (Fig. 15a and b). The rock is light pink to dark-grey in color with medium-to coarse-grains and is made of biotite, hornblende, feldspar and quartz. Biotite flakes appear as small streaks and occasionally in association with hornblende, ilmenite, and titanite. It seems to come from the destabilization of hornblende. It is often included in horblende and plagioclase crystals. Hornblende crystals occurs mainly in two forms: (1) subautomorphic phenocrysts joined with plagioclase in the

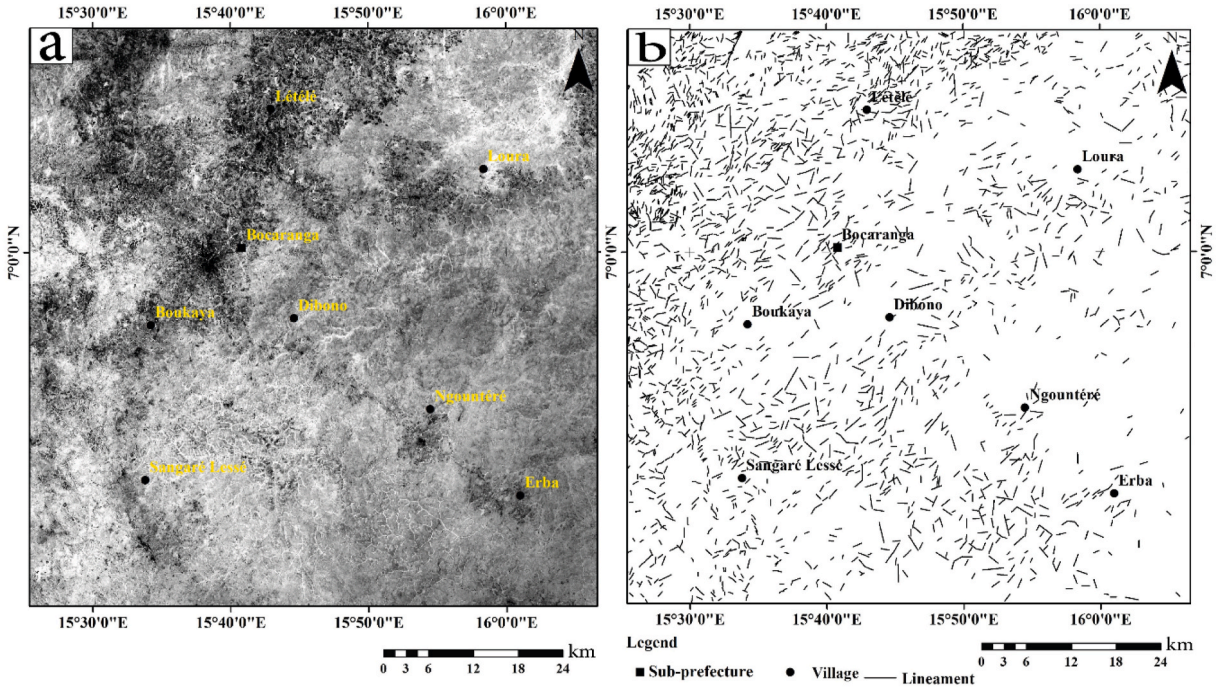

Fig. 7. a) The band 1 (PC1) from panchromatic image; **b)** The lineament synthesis map, obtained from the panchromatic image and the PC1 channel.

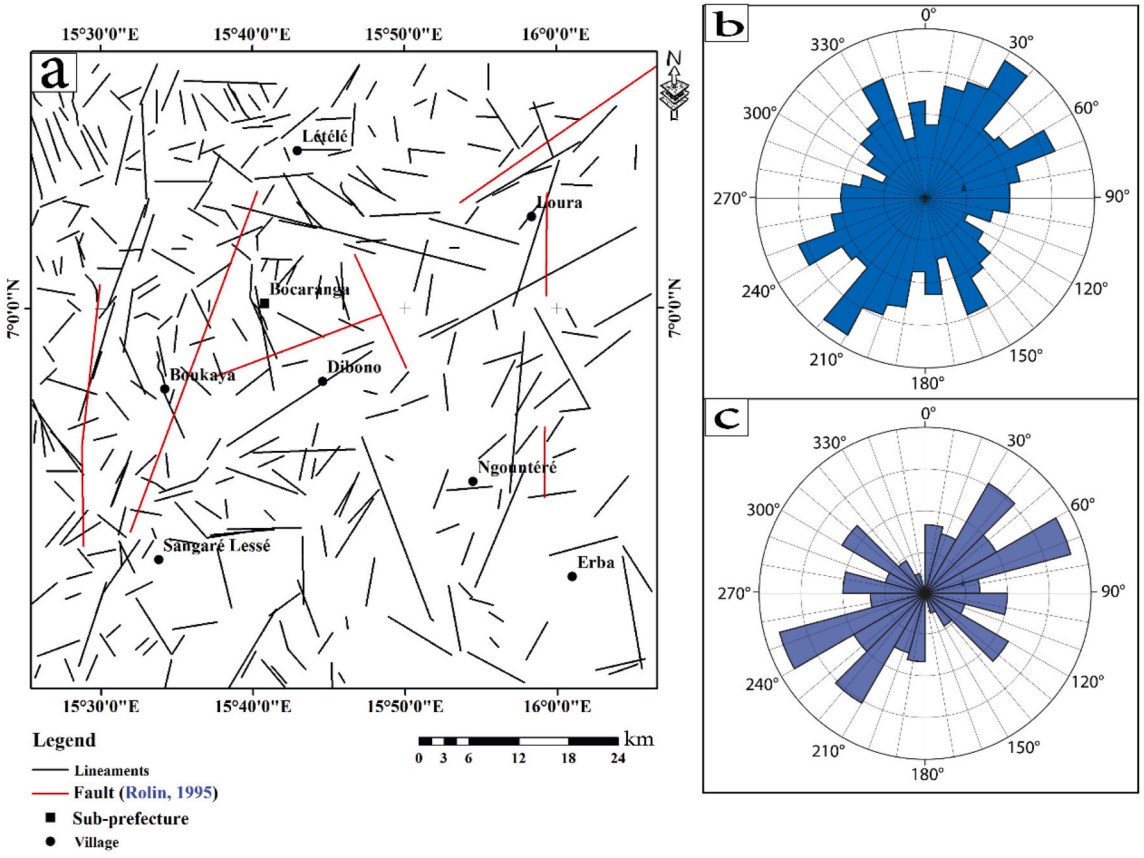

Fig. 8. a) Synthesis map, obtained from the lineament fusion of Lansat 8 OLI and DEM; **b)** Rose diagram of lineaments synthesis of the study area, **c)** The rose diagram of faults, strike-slip, dyke (granitic veins) and pegmatites in the study area.

matrix and (2) xenomorphic grains, which group in aggregates associated with biotite, titanite, epidote, and ilmenite. Some sections of hornblende crystals show a transformation into ilmenite. Plagioclase consists of subautomorphic to xenomorphic crystals. It contains many inclusions (apatite, biotite, and hornblende crystals). Perthite exsolutions are common and granophyres are frequently observed at the

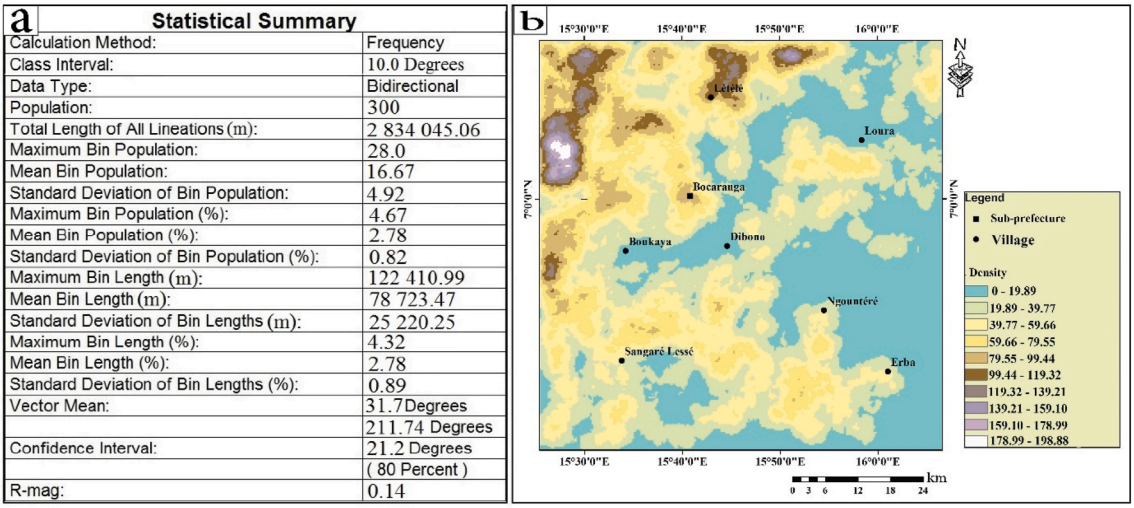

a

Statistical Summary	
Calculation Method:	Frequency
Class Interval:	10.0 Degrees
Data Type:	Bidirectional
Population:	300
Total Length of All Lineations (m):	2 834 045.06
Maximum Bin Population:	28.0
Mean Bin Population:	16.67
Standard Deviation of Bin Population:	4.92
Maximum Bin Population (%):	4.67
Mean Bin Population (%):	2.78
Standard Deviation of Bin Population (%):	0.82
Maximum Bin Length (m):	122 410.99
Mean Bin Length (m):	78 723.47
Standard Deviation of Bin Lengths (m):	25 220.25
Maximum Bin Length (%):	4.32
Mean Bin Length (%):	2.78
Standard Deviation of Bin Lengths (%):	0.89
Vector Mean:	31.7Degrees
	211.74 Degrees
Confidence Interval:	21.2 Degrees
	(80 Percent)
R-mag:	0.14

Fig. 9. a) Summary of statistical data of lineaments synthesis; **b)** The frequency density map of Bocaranga lineaments.

Table 5
Sobel and gradient filter matrices.

Sobel N-S						
1	1	1	2	1	1	1
1	1	2	3	2	1	1
1	2	3	4	3	2	1
0	0	0	0	0	0	0
−1	−2	−3	−4	−3	−2	−1
−1	−1	−2	−3	−2	−1	−1
−1	−1	−1	−2	−1	−1	−1
Sobel E-W						
−1	−1	−1	0	1	1	1
−1	−1	−2	0	2	1	1
−1	−2	−3	0	3	2	1
−2	−3	−4	0	4	3	2
−1	−2	−3	0	3	2	1
−1	−1	−2	0	2	1	1
−1	−1	−1	0	1	1	1
Sobel NE-SW						
0	1	1	1	1	1	2
−1	0	2	2	2	3	1
−1	−2	0	3	4	2	1
−1	−2	−3	0	3	2	1
−1	−2	−4	−3	0	2	1
−1	−3	−2	−2	−2	0	1
−2	−1	−1	−1	−1	−1	0
Sobel NW-SE						
2	1	1	1	1	1	0
1	3	2	2	2	0	−1
1	2	4	3	0	−2	−1
1	2	3	0	−3	−2	−1
1	2	0	−3	−4	−2	−1
1	0	−2	−2	−2	−3	−1
0	−1	−1	−1	−1	−1	−2

borders adjacent to plagioclase. Alkaline feldspar is subautomorphic to xenomorphic. It is represented by orthoclase and microcline. Abundant orthoclase is sometimes perthitic. Quartz occurs in xenomorphic grains with strongly embayed boundaries and occasionally encloses plagioclase and K-feldspar crystals. It frequently forms vermiculated granophyre buds on the rim of feldspar crystals. Titanite occurs as xenomorphic crystals or aggregates of small grains in hornblende. Titanite is sometimes associated with hornblende, biotites, and ilmenite crystals.

Coarse-grained biotite granite (CBG) crops out as slabs in Mbili, Ahnkoné, Zergué, and Colbaya. It is greyish (Fig. 15e–g). It is characterised by an abundance of weakly orientated pink or white rectangular phenocrysts of potassium feldspar with an average size of 2–3 × 1 cm, although individual phenocryst may reach a length of up to 5 cm. The rock has a sharp intrusive contact with the surrounding rocks, late crosscutting occurrences of pegmatite and granite veins. Enclaves are very common in this rock and are dark grey color and fine grained, ranging from a few mm to cm in size, and from ovoid or rounded to narrow streaks in shape. The rock is made of feldspar, quartz, biotite, and accessory minerals such as apatite, zircon, and allanite (Fig. 15h). Biotite flakes contain inclusions of zircon, apatite, and ilmenite. Granophyre sometimes appears on the rim of K-feldspar. Quartz crystals fill microfractures within plagioclase crystals. Titanite is associated to biotite flakes.

Fine-grained biotite granite (FBG) crops out as slabs in Ndouikaré and as aplitic dykes that crosscut migmatitic gneisses in the Kpaïkanya locality (Bocaranga region, Figs. 16a and 18f). It also crops out as slabs, blocks, and balls in the Erémandji locality (Bocaranga region) and as an intrusive rock (NE-SW direction) containing oriented NE-SW gneissic enclaves in the Gaïboula gneisses. In color, the rock is greyish at Erémandji and greyish with reddish flecks and iron oxide clusters at Gaïboula. In Mbili locality (Fig. 15c), FBG outcrops as enclaves within the CBG suggesting that they were emplaced before the CBG. The rock is medium-to fine-grained, equigranular, grainy and feldspar rich (Fig. 16b). The rock consists of feldspars, quartz, biotite, apatite, zircon, allanite, and sericite. Alkali feldspar, widely perthitic and poecilitic is either orthoclase or microcline. It includes quartz, plagioclase, and biotite. Plagioclase includes apatite, oxides, allanite. Biotite flakes show inclusions of zircon, oxide, apatite, allanite, and sphene. Apatite is relatively abundant. Zircon presents a pleochroic aureole in biotite flakes.

Two Mica Granite (TMG) crops out on the right bank of Lima watercourse. It is intrusive in HB-gneiss and amphibolites (Fig. 16c) and exposed as massive and homogeneous rocks in the northern part of the study area. It is medium-and fine-grained, pink to red in color due to the presence of pinkish potassium feldspar and contains enclaves of gneiss and amphibolites. It represents the main lithological unit of the locality of Ngountere where the rock is intersected by late magmatic protodykes, two-mica pegmatite dykes, and dykes. It is also found associated with the FBG in Erémandji.

The rock is (Fig. 16d) made of feldspar, quartz, muscovite, biotite, sericite, and ilmenite. Alkali feldspar crystals are either subautomorphic to xenomorphic orthoclase or microcline. The plagioclase sometimes shows the double albite-Carlsbad twins. Quartz crystallises in the microfractures of feldspar. Muscovite is abundant, in the form of subautomorphic to xenomorphic, colorless flakes. Biotite flakes are less abundant and contain inclusions of apatite and zircon.

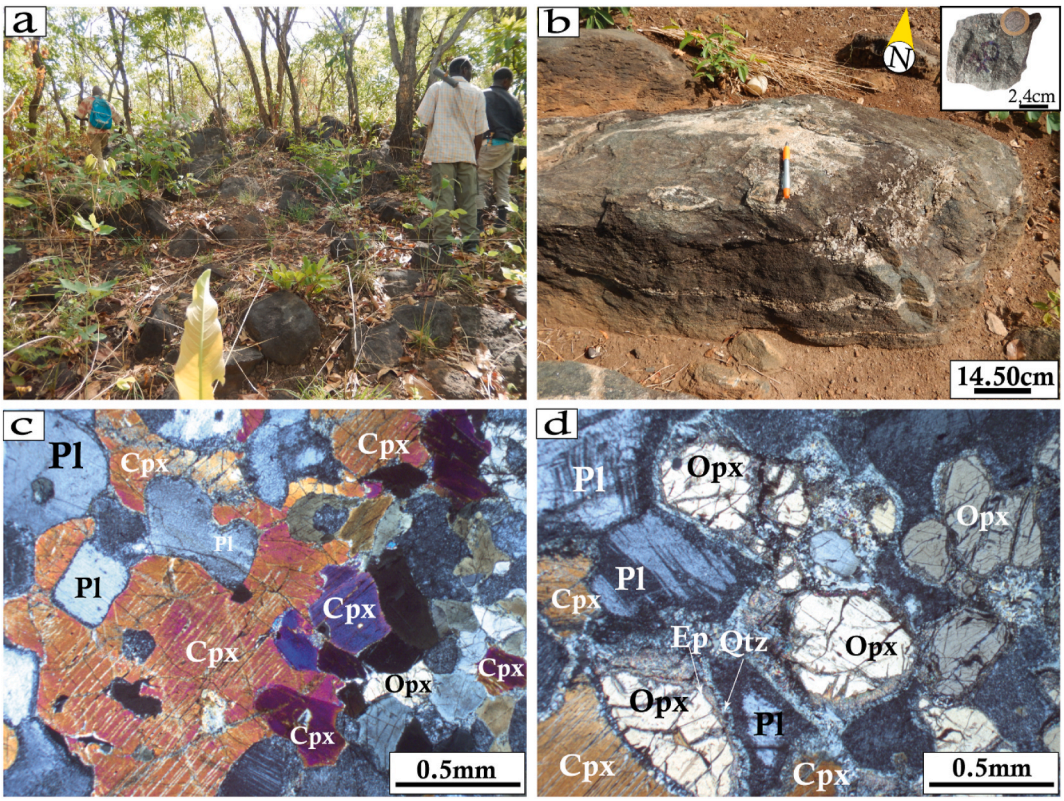

Fig. 10. a and b) Outcrops of amphibole pyroxenites in Kaké locality; **(c and d)** Photomicrographs (crossed polars) of amphibole-pyroxenite. Note the microgranular to coronitic microstructure **(d).**

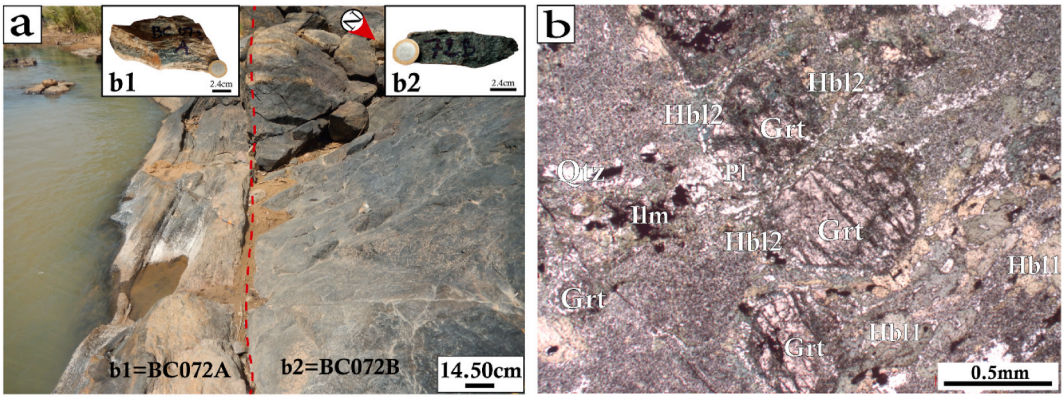

Fig. 11. Field photographs and photomicrographs of representative samples of the Bocaranga showing field relationships, textures and mineralogical composition: **a)** Crops out of the garnet amphibolite (b2 = BC072B) in the bed of the Pendé watercourse, showing its contact with the hornblende-garnet gneiss (HG-gneiss, BC072A) (b1 = BC072A); **b)** In polarized light, the garnet amphibolites (BC072B) are granoblastic in texture. Amphiboles are xenomorphs which surround garnet. In some thin section sections, amphiboles transform into biotite in association with opaque minerals. Op = Opaque minerals. Hbl1 and Hb2 represent the first and second generation of hornblende.

5.1.6. Rock enclaves

They are stretched enclaves including syenodiorite and metadiorite as described below.

Syenodiorite occurs in the hornblende-biotite granite in Dibono (Fig. 13a) and in the coarse-grained biotite granite in Mbili. It is dark grey in color with fine-to medium-grain size. The rock is made of biotite, hornblende, feldspar, quartz, apatite, sphene, and opaque minerals (Fig. 13b). Biotite flakes are automorphic to subautomorphic associated with titanite, opaque minerals (ilmenite), and hornblende crystals. Hornblende crystals, subautomorphic to xenomorphic, show some crystals tranformed into titanite and ilmenite. Apatite, titanite, biotite and ilmenite are included in hornblende crystals. Plagioclase crystals are subautomorphic, zoned (marked by preferred alteration of the center of the crystal). Alkali feldspar is subautomorphic to xenomorphic orthoclase. Titanite is automorphic to xenomorphic (occurring as small grains on the borders of ilmenite grains) crystals associated with hornblende, biotite, and opaque minerals. Ilmenite is abundant in rock.

Metadiorite occurs in coarse-grained biotite granite, and hornblende biotite granite. Fine-grained and foliated, it is characterized by its dark-grey color and various shapes (elliptical, elongated, rounded and sometimes angular (Fig. 13c)) parallel to the mineral preferred orientation in HBG, CBG and migmatites. It has grano-nematoblastic texture (Fig. 13d) and is composed of abundant hornblende, plagioclase, and interstitial minerals: quartz, biotite, epidote, titanites, and ilmenite.

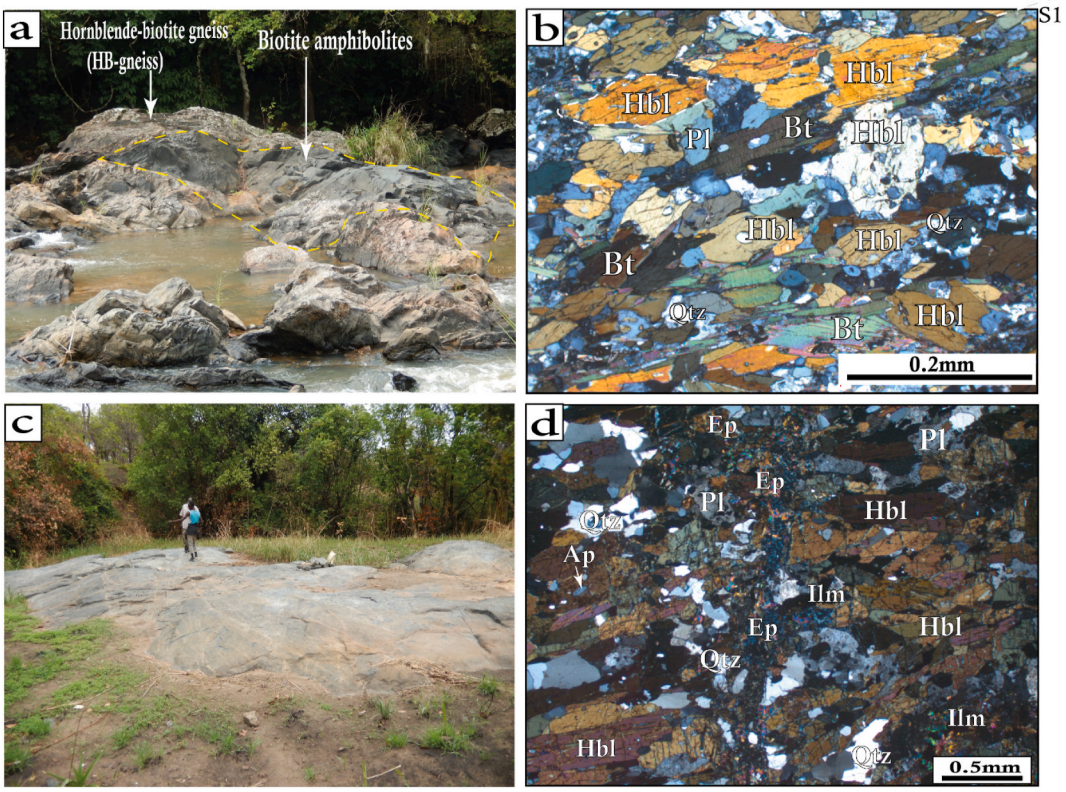

Fig. 12. Field photographs and photomicrographs of representative samples of the Bocaranga showing field relationships, textures and mineralogical composition: **a, b)** Biotite amphibolite enclave in hornblende-biotite gneiss (HB-gneiss). In cross polarized light, the biotite amphibolite show a grano-nemato-lepidoblastic texture; **c, d)** Crops out of epidote amphibolites; In cross polarized light, they show a nematoblastic texture.

Hornblendes have subautomorphic to xenomorphic sections. Some crystals are in association with titanite and ilmenite. Plagioclase is subautomorphic to xenomorphic. It contains inclusions of hornblende and biotite crystals. Biotite is subautomorphic or xenomorphic lamellar, of variable size. It would come from the destabilization of hornblende crystals. It is generally chloritized. Biotite is in inclusion in hornblende and plagioclase crystals. Quartz is xenomorphic and occurs as small grains between hornblende crystals of the porphyroid facies.

5.2. Structures and deformation phases

In the study area, rocks are more or less deformed. They are characterized by magmatic and gneissic foliation, shear planes, folds, magmatic and mineral lineation, and boudins. Foliation is used as a descriptive term for any penetrative planar feature that occurs in rocks. In the following sections, we refer to the foliation as ''S'' with the same indices for the associated deformation phase. Magmatic foliation, observed in granites from Dibono and Bocaranga (Hankoné and Mbili) is characterized by preferred orientation of euhedral to subhedral crystals: perthitic k-feldspar phenocrysts, plagioclase, and amphibole (Fig. 17a, 18a-c) acquired during the magmatic stage or later.

The gneissic foliation (Fig. 18d–g) is observed in hornblende garnet gneiss from Kaké (Dibono, Pendé River), Dibono, Ngountéré and Loura and in biotite amphibolite from Dibono. It is characterized by the alternation of dark and white bands. It is represented by early NW-SE trending foliation that has been progressively rotated parallel to S2 foliation observed in the hornblende garnet gneiss and hornblende biotite granites as well. The S1 foliation is sub-perpendicular to the S2 foliation. The S1 foliation strikes N132°E - N160°E with moderate dips (40–50°) towards North-East and South-West partially or completely transposed by NW-SE to NE-SW S2 foliation, the most important and predominant in the Bocaranga locality. Lower hemisphere projection diagrams (Fig. 20) indicate 63/42 as the best pole. This transposition leads to the development of S2 foliation in migmatitic gneisses. The syn-migmatitic foliation is underlined by the alternation of melanosome and leucosome (Fig. 13c).

In the hornblende biotite gneiss and hornblende garnet gneiss, S2 foliation (Figs. 17b and 18h) appears as the result of the transposition of previous S1 foliation. This foliation strikes NE–SW with moderate dips (33–65°) toward NW, on the lower hemisphere projection diagrams, indicating 114/52 and 141/43 as best poles (Fig. 20).

In Loura, (northeast Bocaranga), the hornblende biotite granite is strongly oriented and shows a magmatic S2 foliation with NE–SW strikes and high dips 60–80° toward the NW or SE. In the hornblende biotite granites, the S2 foliation is defined by biotite flakes, K-feldspar crystals, mica flakes, and platy quartz (Fig. 17a). The distribution of S2 foliation from the main outcrops in the axial part (Dibono-Loura) of the study area shows a girdle distribution. Their planes have moderate to high dips predominantly to the Northeast. The angle between S2 and C2 points to mylonitisation of hornblende biotite granites (Fig. 17a). In Dibono, hornblende biotite granites shows preferred orientation of alkali feldspar megacrystals with NE–SW strikes and moderate to high dips 41–72° toward the NW or SE (Figs. 13a and 20).

The S3 foliation is typically a deformation of superimposed folding. The structures associated with this deformation are the result of the transposition and reorientation of the S2 structures (Fig. 18b–f). The S3 foliation overprinted the pre-existing S2 foliation. The S3 planes are equally distributed; they trend N50-80°E with a moderate to high dip (40–70°) toward the NW and SE (best pole is at 147/50). S2 and S3 strike NE-SW direction.

In the coarse-grained biotite granite, S3 magmatic foliation strikes from NE-SW to ENE–WSW with moderate to high dips (45–70°) toward the NNW (Fig. 18b and c). The lower hemisphere projection diagrams show an organization of foliation poles in the Northwestern frame with

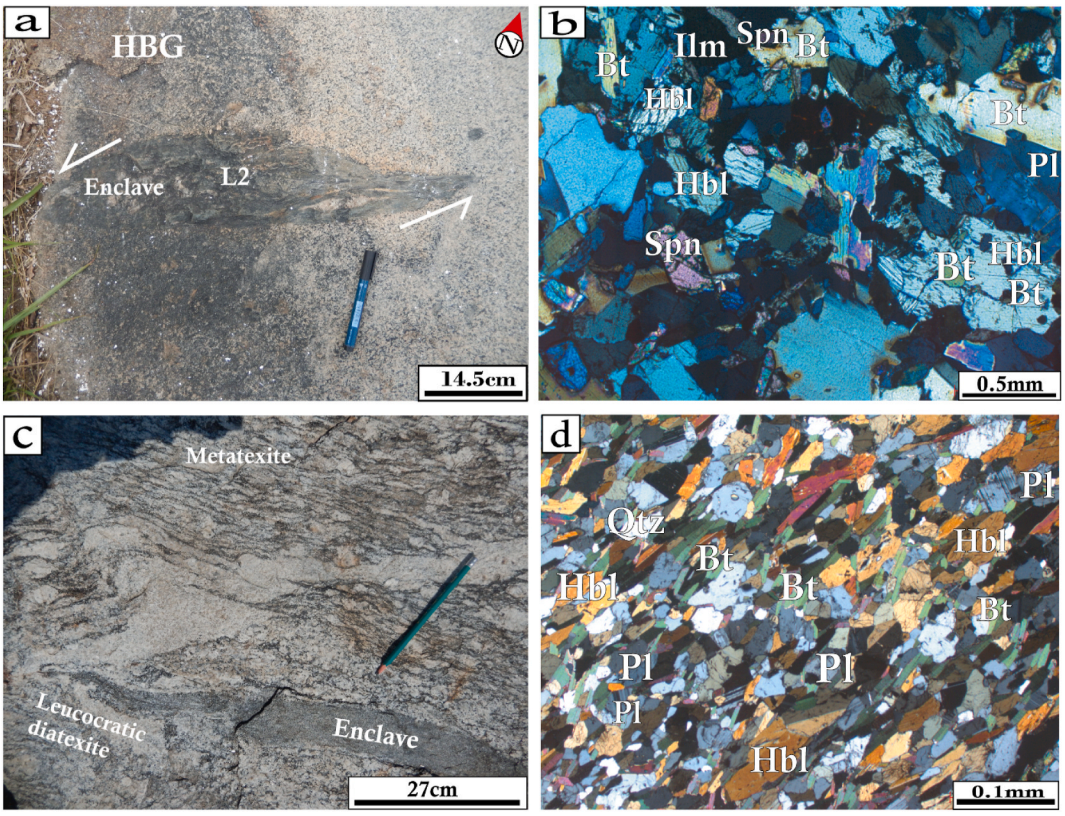

Fig. 13. Field photographs and photomicrographs of representative samples of the Bocaranga showing field relationships, textures and mineralogical composition: **a, b)** Syenodiorite enclave in hornblende-biotite granites (HBG). In cross polarized light, the syenodiorite enclave exhibit a microgranular texture. They are rich in inclusion of plagioclase from HBG; **c)** Migmatite outcrops show metadiorite enclaves in the locality of Colbaya**; d)** In cross polarized light, the metadiorite enclaves show a lepido-nematoblastic texture.

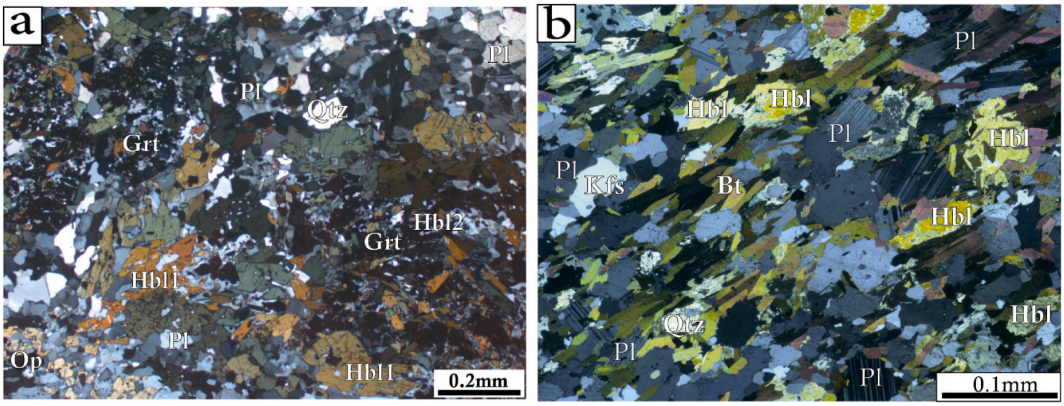

Fig. 14. Photomicrographs of samples of the Bocaranga showing textures and mineralogical composition: **a)** In cross polarized light, the hornblende-garnet gneiss (HG-gneiss, BC072A) have a grano-nematoblastic texture. The amphiboles occur as aggregates and are sometimes intercalated between feldspars which are oriented almost parallel to the foliation of the rock; **b)** In cross polarized light, the hornblende-biotite gneiss show a lepido-nematoblastic texture. Hbl1 and Hb2 represent the first and second generation of hornblende.

the best poles at 125/46 and 174/48 (Fig. 20).

F1 fold is identified in hornblende biotite gneiss and biotite amphibolite. It is represented by the axial plane parallel to the S1 foliation (best line at 144/48, Figs. 18e and 20). The S1 foliation is folded by deformation accompanied by the development of F2 similar and asymmetric folds (best lines are at 219/14–40/10, Fig. 20) which show axial planes concordant to the S2 schistosity marked by the preferred planar orientation of amphibole and biotite (Fig. 18g, and h).

The F3 folds (best line 250/20, Figs. 18d and 20) result of the development of later folds across the earlier structures. It is asymmetric Z-shape (Fig. 18d).

The mineral lineation is defined by preferred orientation of automorphic or subautomorphic hornblende minerals (Fig. 18b–d) in hornblende biotite granite by acicular hornblende crystals on the S2 magmatic foliation planes such as magmatic lineation in Dibono locality and the central part of Yadé massif. This lineation strikes NE–SW with low to moderate plunges (20–55°) towards SW. The stretching lineation is characterized by deformed, constricted grains of minerals such as quartz ribbons and biotite flakes commonly expressed on foliation planes in hornblende garnet gneiss and hornblende biotite gneiss. In

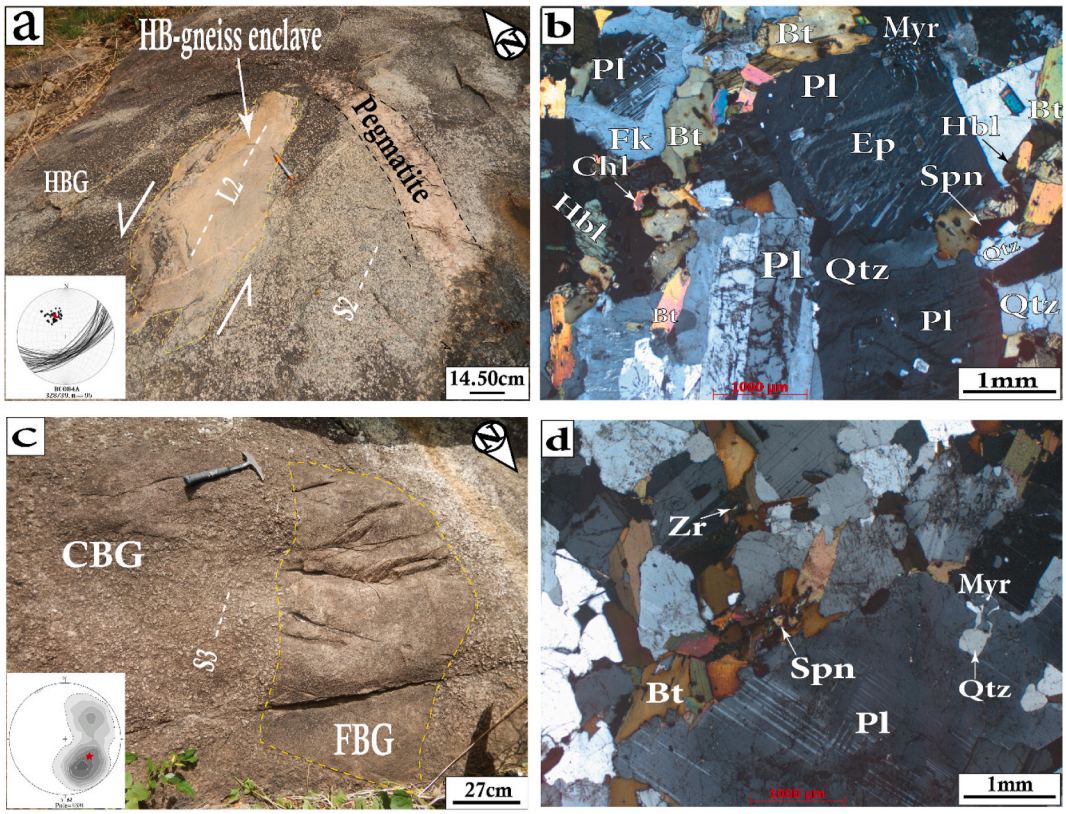

Fig. 15. Field photographs illustrating the crops out mode of the Bocaranga: **a)** Crops out of hornblende-biotite granitoide (HBG) slab and intrusive in the gneiss within which spindle-shaped enclaves of gneiss appear. They are cut by quartz vein and pegmatite; **b)** In cross polarized light, the HBG shows granular porphyroid texture. The presence of myrmekites in some thin–sections indicates the transition between magmatic and sub–magmatic textures; **c)** Crops out of CBG presents on the edge an enclave of FBG; **d)** In cross polarized light, the CBG has a granular texture to porphyroids.

gneiss, lower hemisphere diagrams show the best lines at 218/12 and 241/19 (Fig. 20).

The magmatic lineation refers to the organization of millimetric to decimetric long axis of lens-shaped or elongated enclaves (syenodiorite and metadiorite) in hornblende biotite granites (Figs. 13a, 15a and 18a). These enclaves are aligned parallel to the preferred orientation of alkali feldspar megacrystals with low-to moderate-plunges (30–50°) toward SW.

B2 asymmetric boudins are developed in hornblende biotite gneiss (Fig. 17c). According to Ghosh and Ramberg (1976); Hanmer (1986) and Goldstein (1988), these boudins are typical for shear zones. The asymmetric aspect shows that they are pre-to syn-shearing (Goldstein, 1988) boudins, with the initial layers trending oblique to the shear zone. C2 shear zones appear as ductile zones which sheared the S1 foliation (Fig. 17c). Locally, it gives to amphibolites or gneisses a strong tectonic banding by transposition of the previous S1 foliation.

In this study, σ–type kinematic markers are structures linked to rigid objects in the mylonitic matrix (Fig. 17a–c, and 18c). The shape of this structure is controlled on one hand by the coupling of the object and the matrix and on the other hand by the shearing deformation gradient in shear planes.

Cross section AB (Fig. 19) presents foliation planes having substantially the same direction, with NW or SE dips. These planes of folds with low plunges. The poles of the foliation planes are organized around the same great circle.

5.2.1. Kinematic indicators

Kinematic analysis involved measurements of mineral lineations, foliation planes and S-C foliations (17a-b, and 18c), as well as determination of shear sense based on the interpretation of asymmetric structures. Hornblende fish (Fig. 12b) commonly elongated parallel with the S1 foliation, asymmetric boudins (Fig. 17c and 18f), asymmetrical feldspar prophyroblasts (Fig. 17a–c), asymmetrical folds (Fig. 17c and 18d-h), are good shear sense indicators and define a predominantly sinistral sense of shear, although locally dextral displacements may also occur. The shear zone is also marked by strike-slip faults with sinistral sense of shear movement (Fig. 18a). Other minor shear zones concordant with the ENE–WSW-trending S3 subvertical foliation crosscut the S2 subvertical foliation and they displays sinistral kinematics. The shear zone is marked also by indicators such as S-C structures (Fig. 17a–c, and 18b-f), and asymmetry of F3 folds, which are good shear sense indicators. The sinistral sense of movement along the shear plane was also deduced from displacement of quartz veins and hornblende prophyroblasts, some of which show rotational movement (Fig. 17c).

6. Discussion

In this study, the different rock types of Bocaranga area, are mapped using Landsat image by developing FCC images, principal component, and band ratios images. The band ratios images best discriminated the rock types of the region when compared to the results of the FCC and PCA images. The boundaries of the lithological units were determined by correlating the Landsat 8 satellite images, the existing CAR geoligical map of Rolin (1995), and using field observations and laboratory data. The study allowed us to provide a lithological sketch map of Bocaranga area (Fig. 20). The results of FCC developed using the bands 7, 6, and 5, and the RGB compositions of the principal components PC1, PC3, and PC4 and the band ratios 7/4, 7/3, 6/3, and 7/4, 6/3, 5/7 are well integrated. The lineaments that were mapped using the Sobel's directional filters and extraction of the six different azimuth angles (90°, 135°, 225°, 270°, 315°, and 348°) in the Landsat images 8 OLI and SRTM-DEM enabled this study to compare them to those of the field observations

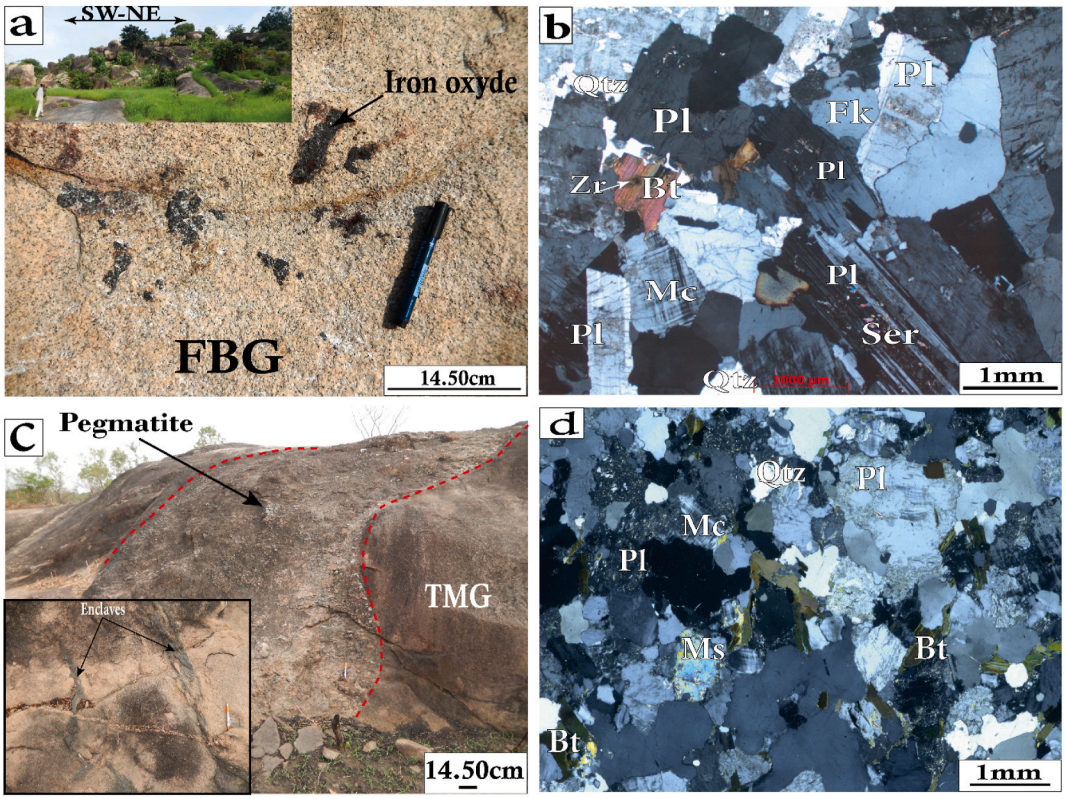

Fig. 16. Field photographs and photomicrographs of different rock–types in the Bocaranga aera; **a)** FBG is massive, fine to medium-grained, and free of any planar texture; **b)** In cross polarized light, the FBG show granular textures; **c)** TMG is exposed as massive and homogeneous rocks. Pegmatitic dyke crosscutting the TMG; **d)** In cross polarized light, the TMG shows a granular to heterogranular texture.

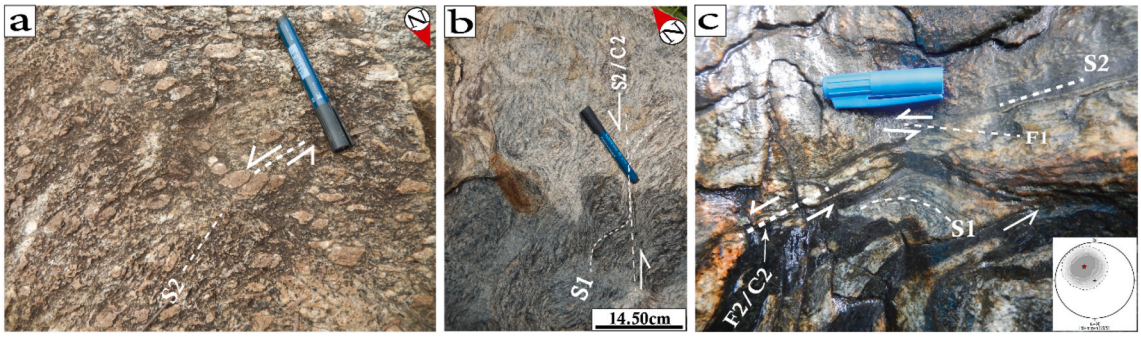

Fig. 17. Field photographs showing various deformation features within the granitoids and the basement rocks of Bocaranga pluton: **a)** Orthogneissified porphyritic granite (HBG) of Loura with S-C structures; **b)** S1 foliation of mean direction 64/40 in the gneiss partially transposed to S2 (SW-NE) foliation concordant with sinistral shear zone (C2); **c)** Asymmetric boudins indicating the sinistral shear in gneiss of Colbaya; note the C2 shear planes.

with the aim to produce a lithostructural map of Bocaranga (Fig. 20).

The lineament map obtained shows 1085 lineaments with lengths varying between 0.40 and 3.80 km and an average at 0.91 km. According to Fig. 9, the total population of lineaments is 300 for a total length of 2,834,045.06 m. The directional analysis of lineaments (Fig. 8a–c) showed the occurrence of lineaments with directions varying between the NE-SW and NW-SE with dominance of N30°- N40°E direction followed by N60°-N70°E and N150°-N160°E directions. These directions are also represented by foliations, faults, boudins, mineral lineation, quartz veins, and dykes (granitic) (Fig. 8c). The central part of the study area and the localities of Létélé and Ngountéré are mainly affected by NW-SE and NE-SW ductile shear zones, which are predominantly represented by numerous sinistral ductile S/C structures. The lineament synthesis map reveals that the Létélé locality, the northwestern Bocaranga and the southwestern Boukaya are high density lineament areas (Fig. 9b). These lineaments are parallel to the trace of the Mbéré shear zone (MBSZ) that seems to be the northeastern prolongation of the Central Cameroon Shear Zone and seems to be linked to the same tectonics that developed the Central Cameroon shear zone (CCSZ; Fig. 1a and b, 8a-b).

6.1. Structural evolution of the Bocaranga area and links with regional deformation of the Central African Orogenic Belt (CAOB)

Structural studies show five main ductile structures (foliations, folds, mineral lineations, shear zones, and boudins) recorded by metamorphic and magmatic rocks. These structures are foliations; folds; mineral lineations; boudin, and shear zones, and are related to the D1 deformation (S1, F1), and D2 (progressive deformation: from S2, F2, L2, C2, B2 to S3, F3, L3, C3) deformation stages according to the relative chronology. The

Fig. 18. Field views of main structural elements on Bocaranga area: **a)** S2 magmatic foliation in the HBG of Dibono. Note the sinistral strike-slip fault in the HBG; **b)** Magmatic foliation in the Hankoné CBG (Bocaranga center). Note the parallelism of the alkaline feldspar crystals with the enclave and the sinistral strike-slip fault in the CBG; **c)** Orthogneissified porphyritic granite of Béféré (CBG, Bocaranga center) with S-C structures; **d)** The asymmetric shape "S" of F3 folds with S3 foliation subparallel to the axial plane of the fold; **e)** Sn foliation and Fn fold in biotite amphibolites. It has an average orientation 63/42; **f)** Sn+1 foliation of mean direction 133/39 in the gneisses transposed to Sn+2 (WSW-ENE) foliation concordant with sinistral shear zone (C3); **g)** Asymmetric boudins indicating the dextral shear in HB-gneiss of Dibono. Note the C2 shear planes; **h)** F2 folds in the HB-gneiss of Ngountéré.

tectonic evolution ends with the D3 deformation which is characterized dominantly by brittle structures (mainly fractures). The age of the various deformations in the region of Bocaranga remains an important problem. The D1 event is only recorded in the metamorphic rocks (amphibolites and gneiss) and it is associated to the development of a S1 foliation and asymmetric F1 folds. D2 event is well-recorded in both the magmatic and metamorphic rock units. It is characterized by a heterogeneous deformation that affects the previous D1 fabric. D2 is accompanied by a progressive migmatitization which outlasted D2 deformation. The lack of the D1 imprint in granitoids (HBG, FBG, CBG and TMG) indicates that their emplacement post-dates this deformational phase.

D2 phase is related to sinistral movements along NE-SW to ENE-WSW oriented shear zones. The NE-SW direction is recorded in the hornblende biotite granite and the ENE-WSW direction in the coarse-grained biotite granite. Two rock types are distinguished: dominant biotite granite and hornblende-biotite granite characterized by equant porphyritic texture with megacrysts of K-feldspars. Microgranular mafic magmatic enclaves are locally observed. The preferred direction NE-SW represented in the whole of the investigated Bocaranga area, would be

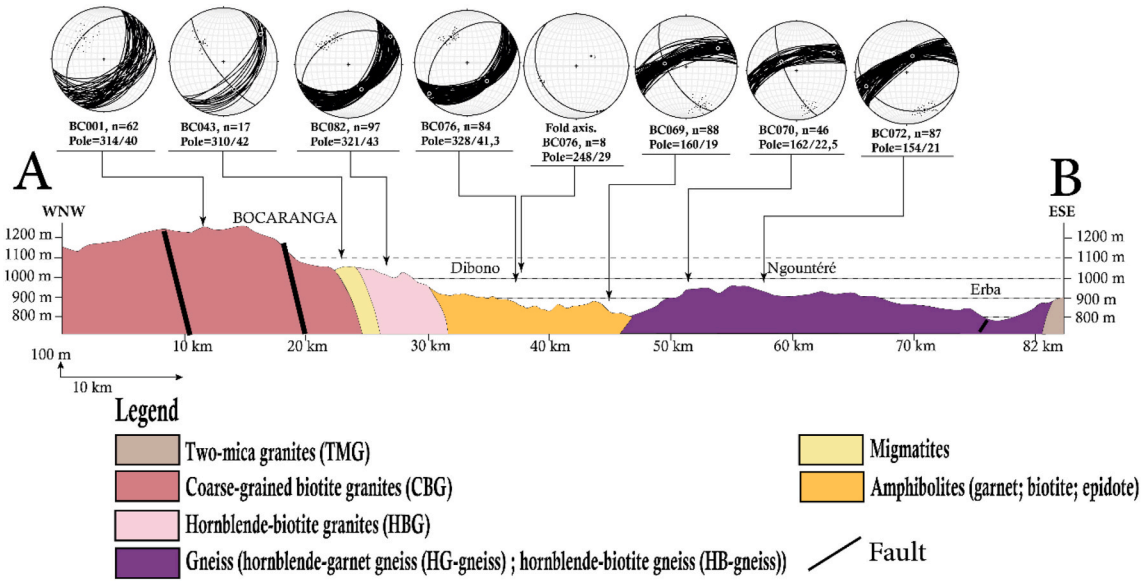

Fig. 19. Lithostructural section showing the relationships between the lithological units of Bocaranga. Location of the cross-section is indicated in Fig. 20.

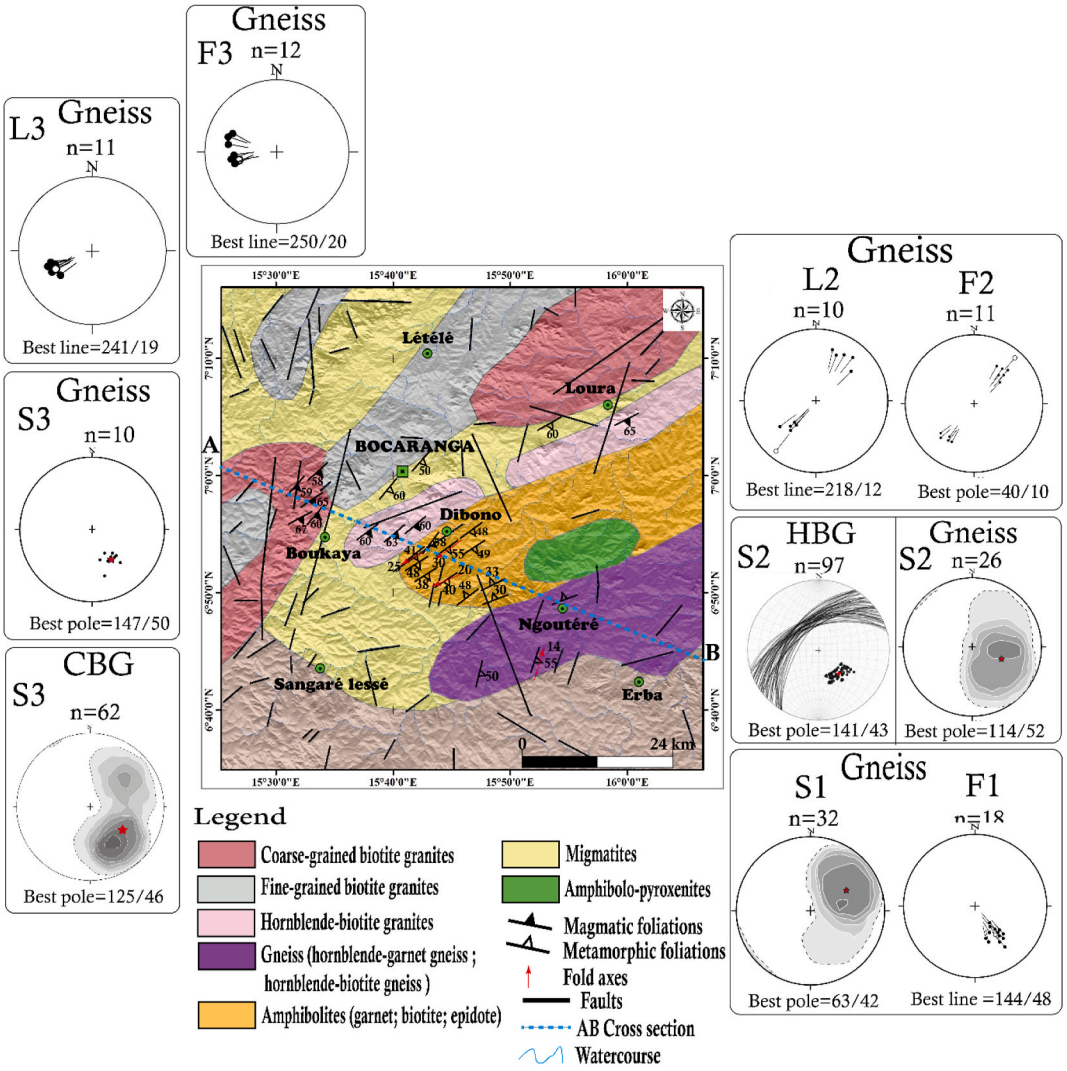

Fig. 20. Litho-structural map of Bocaranga. CBG=Coarse-grained biotite granites; HBG=Hornblende-biotite granites.

linked to the general S2 and S3 foliations that developed during the second phase of ductile deformation (D2).

The S1 metamorphic foliation observed in banded gneisses and amphibolites is the oldest structure, with a main orientation of NW-SE. This S1 metamorphic foliation is transposed by F2 folds and C2 shear planes with the development of NE-to NW-directed S2 metamorphic foliation along these axial and shear planes. This S2 planar structure bears a gentle to steep SSW-NNE plunging mineral lineation (L2). The asymmetry of F2, F3 folds with "S" shapes in banded gneisses (Fig. 18d–h) and amphibolites (Fig. 18g) is consistent with a sinistral sense of shear movement as already proposed by Ngako et al. (2003, 2008) and Mapoka et al. (2011) for the CCSZ or MBSZ kinematics during the regional D2 shear phase. The parallelism between L2, L3 mineral lineation and the F2, F3 fold axes, respectively, suggests that simple shear caused the folding. The boudins have an asymmetric (Fig. 17c), rhomb to lens shape and shape with tapering wings that is consistent with shear band boudins (Swanson, 1992; Goscombe and Passchier, 2003). Their asymmetric shapes suggest simple shear with sinistral sense of shear movement.

In the Bocaranga granitic plutons, the NE-SW direction of S2, S3 magmatic foliations and L2, L3 mineral lineation are subparallel to the homogeneous NE-SW trend shown by the S2, S3 metamorphic foliation, L2, L3 mineral lineation, F2, F3 folds, C2, C3 shear planes (Fig. 18f) and B2 boudins in the country rocks. Some kinematic markers identified within granites include S-C fabric and σ-type feldspar phenocrysts (Figs. 17c and 18c), both showing sinistral shear motion. These structures identified in the plutons and country rocks are attributed to the sinistral sense of shear phase (D2) and are consistent with sinistral sense of shear movement during emplacement of the Bocaranga granitic plutons. The scarcity of structure orientation in the TMG and FBG (except the contact zones), would imply that these granites would have crystallized in the absence of any stress. It follows from the above remarks that the emplacement of the Bocaranga granitic plutons started in the context of regional transpressional regime and ended in the absence of deformation.

D3 is a phase of brittle deformation with sub-vertical fractures and regional–scale faults. These fractures show three main directions (Fig. 8c), all corresponding to the main direction of the shear zones in the Northern domain of CAR and also in the Central domain of Cameroon: 1) N30-45°E corresponds to the directions of Mbéré shear zone (Fig. 1a) that is the prolongation of one branch of the Cameroon Central shear zone (Fotouni-Fondjomekwet shear zone; Tcheumenak et al., 2014); 2) N60 - 75°E equivalent to Bozoum-Ndélé shear zone (Mapoka et al., 2011; Topien, 2012) that is the prologation of the Sanaga shear zone (Moreau et al., 1987; Ngnotué et al., 2000); 3) N120 - 135°E also found in the southern part and the eastern part of the central domain (Tombel and Banyo basements) of Pan-African fold belt and interpreted as traces of the Benue trough (Nzenti et al., 1988; Ngnotué et al., 2000; Njome and Suh, 2005). This phase of the emplacement of the massif would be marked by an important circulation of fluids responsible of the presence of pegmatites veins (Fig. 16c).

The Bocaranga granitoid structures testify the sinistral sense of shear movement during the deformation along the CCSZ. It is also similar to that of the Bossangoa-Bossembele Shear Zone where Mapoka et al. (2011) and Danguene et al. (2014) attributed the sinistral sense of shear movement to the D2 deformation phase coeval the emplacement of the Tamkoro-Bossangoa plutons. It is also similar to that of Tcholliré-Banyo Shear Zone where Nomo et al. (2017) attributed the sinistral sense of shear movement to the D2 deformation phase coeval to the emplacement of the Tcholliré plutons.

The kinematic evolution of the Bocaranga area is rather different to that of (i) Fambélé Garoua-Boulaï area in west Central African Republic, (ii) Magba Shear Zone in Cameroon (Ntieche et al., 2017), and (iii) Ndiéki area in Cameroon (Awoum Julios et al., 2020), according to which the early kinematic phase is a dextral shear phase (D2) followed by a sinistral shear phase (D3) during the development of these shear zones. This difference in the deformation chronology is probably due to the complexity of the CCSZ kinematics (Ngako et al., 2003, 2008; Njonfang et al., 2006, 2008; Dawaï et al., 2017).

We propose from the above observations that the emplacement and deformation of the Bocaranga granitic plutons were initiated during Pan-African D2 phase (responsible for sinistral shear movement).

The structural evolution in the Bocaranga segment of MBSZ or CCSZ system began with ductile deformation and ended with brittle deformation. This is a classical feature of ductile shear zones that was subsequently overprinted by a brittle event (Passchier et al., 1993; Tchankam et al., 1997; Suh and Dada, 1997; Passchier and Trouw, 1998), although shear zones in which macroscopically brittle deformation predates a ductile event have also been described (Imber et al., 2001). The elongate shape of the plutons, variable orthogneissification and foliation strikes parallel to the CCSZ point to syntectonic magma emplacement.

These results imply a syntectonic emplacement of the Bocaranga pluton along a sinistral simple shear zone. This syntectonic emplacement in sinistral shear regime is related to deformations along the Central Cameroon Shear Zone (CCSZ) also known as the Adamawa shear zone (ASZ, Njanko et al., 2006).

Pan-African ages (615–650 Ma) have been obtained on plutonic rocks in the western part of the CCSZ (Nguiessi Tchankam et al., 1997; Njiosseu et al., 2005; Nomo et al., 2017) and in NE-SW trending ductile shear zones in Adamawa, just west of the study area (Nzenti et al., 2006). The similarity between these dated plutons and the ones we have described in Bocaranga area allow us to constrain the age of emplacement to the Pan-African (615–650 Ma).

7. Conclusion

Using Landsat 8 OLI and SRTM-DEM images, detailed petrographic and field structural observations, this paper provides new results which help to highlight (i) the polyphase deformation of the study area and (ii) the emplacement mechanism of the Bocaranga pluton. FCC, band Rationing and the selective principal component analysis associated to image processing of the satellite data and the field data showed the occurrence and spatial distribution of different petrographic units within the study area. The study of Sobel directional filters and extraction of six different azimuth angles and spectral enhancement allowed lineament extraction.

Structural and kinematic analyses show three deformation phases and a syntectonic emplacement of the Bocaranga pluton during D2 sinistral sense of shear. This syntectonic emplacement in sinistral sense of shear movement is related to deformations along the Mbéré shear zone or the CCSZ.

Based on knowledge of regional Pan-African deformation history within the COAC in Central African Republic, we can state that the emplacement of the Bocaranga pluton was initiated during regional D2 deformation. The scarcity of structure orientation in the TMG and FBG could imply that these granites would have crystallized in the absence of any stress.

The tectonic evolution in the Bocaranga segment of the MBSZ or CCSZ system began with ductile deformation and ended with brittle deformation. This is a classical feature of brittle-ductile shear zones.

The elongate shape of the plutons, variable orthogneissification and foliation strikes parallel to the CCSZ point to syntectonic magma emplacement.

These results imply a syntectonic emplacement of the Bocaranga pluton along a simple shear in sinistral sense of shear movement related to the deformations along the CCSZ.

Declaration of competing interest

The authors declare that they have no known competing financial interests or personal relationships that could have appeared to influence

the work reported in this paper.

Data availability

No data was used for the research described in the article.

Acknowledgements

This study is a part of the Ph.D. work of the first author. The authors thank University of Bangui and R.TOPIEN 4D production studio for financial support of the fieldwork in the Central African Republic. We thank France Embassy in Central African Republic for providing scholarships and financial support for six months to perform the analytical work of thesis project at GeoRessources laboratory of the University de Lorraine-CNRS, Nancy, France. Thanks to Cedric Demeurie for his help in the preparation of thin sections. The anonymous reviewer and Editor-in-Chief are sincerely thanked for careful and constructive comments which significantly improved this manuscript.

References

Abrams, M.J., Rothery, D.A., Pontual, A., 1988. Mapping in the Oman ophiolite using enhanced Landsat thematic mapper images. Tectonophysics 151 (1–4), 387–401.

Awoum Julios, Efon, Eric Martial, Fozing, Maurice, Kwékam, Kouémo Jules, Tcheumenak, Kana Styve Cliff, Choumele, Achu Megnemo Ludovic, 2020. Structural characterization of the Pan-African Ndieki area in the Foumban-Bankim shear zone (west Cameroon): constraints from field observations and microstructures. Arabian J. Geosci. 13 (17), 1–16.

Bessoles, B., Trompette, R., 1980. La Chaîne Pan-Africaine "'zone Mobile d'Afrique Centrale (Partie Sud) et Zone Mobile Soudanaise. Mémoire B.R.G.M 92, 326.

Boulvert, Y., 1995. Carte Géomorphologique de La République Centrafricaine. Institut Français de recherche scientifique pour le développement en Coopération.

Brown, Michael, 1973. The definition of Metatexis, Diatexis and migmatite. PGA (Proc. Geol. Assoc.) 84, 371–IN2.

Caby, R., Sial, A.N., Arthaud, M., Vauchez, A., 1991. Crustal evolution and the Brasiliano orogeny in northeast Brazil. In: Dallmeyer, R.D., Lécorché, J.P. (Eds.), The West African Orogens and Circum-Atlantic Correlatives. Springer, Berlin, Heidelberg, pp. 373–397. https://doi.org/10.1007/978-3-642-84153-8_16.

Cordani, U.G., D'Agrella-Filho, M.S., de Brito-Neves, B.B., Trindade, R.I.F., 2003. Tearing up Rodinia: the neoproterozoic palaeogeography of south American cratonic fragments. Terra. Nova 15 (5), 350–359.

Cornacchia, M., Dars, R., 1983. Un trait structural Majeur Du continent Africain; Les lineaments Centrafricains Du Cameroun Au Golfe d'Aden. Bull. Soc. Geol. Fr. S7-XXV (1), 101–109. https://doi.org/10.2113/gssgfbull.S7-XXV.1.101.

Crippen, Robert Edward, 1989. 'Development of Remote Sensing Techniques for the Investigation of Neotectonic Activity, Eastern Transverse Ranges and Vicinity, Southern California'. PhD Thesis. University of California, Santa Barbara.

Danguene, P.E.Y., Ngnotue, T., Ganno, S., Biandja, J., Kankeu, B., Nzenti, J.P., 2014. Paleoproterozoic synkinematic Magnesian high-K magmatism from the Tamkoro-Bossangoa massif, along the Bossangoa-Bossembele shear zone in north-western Central African Republic. J. Geosci. Geomatics 2 (4), 151–164.

Das, Sumit, Pardeshi, Sudhakar D., Kulkarni, Pallavi P., Doke, Arjun, 2018. Extraction of lineaments from different azimuth angles using Geospatial techniques: a case study of Pravara basin, Maharashtra, India. Arabian J. Geosci. 11 (8), 160. https://doi.org/10.1007/s12517-018-3522-6.

Dawaï, Daouda, Tchameni, Rigobert, Bascou, Jérome, Wangmene, Salomon Awe, Martial Fosso Tchunte, Périclex, Jean-Luc Bouchez, 2017. Microstructures and magnetic fabrics of the Ngaoundéré granite pluton (Cameroon): implications to the late-Pan-African evolution of Central Cameroon shear zone. J. Afr. Earth Sci. 129, 887–897.

Dumont, J.F., 1986. Identification Par Télédétection de l'accident de La Sanaga (Cameroun). Sa Position Dans Le Contexte Des Grands Accidents d'Afrique Centrale et de La Limite Nord Du Craton Congolais. Geodynamique 1, 13–19.

Fossen, Haakon, Harris, Lyal B., Cavalcante, Carolina, José Archanjo, Carlos, Ávila, Carlos F., 2022. The Patos-pernambuco shear system of NE Brazil: partitioned intracontinental transcurrent deformation revealed by enhanced aeromagnetic data. J. Struct. Geol. 158, 104573.

Gad, Sabreen, Kusky, Timothy, 2006. Lithological mapping in the eastern Desert of Egypt, the Barramiya area, using Landsat thematic mapper (TM). J. Afr. Earth Sci. 44 (2), 196–202.

Ganwa, A.A., Klötzli, U.S., Hauzenberger, C., 2016. Evidence for Archean inheritance in the pre-Panafrican crust of Central Cameroon: Insight from zircon internal structure and LA-MC-ICP-MS UPb ages. J. Afr. Earth Sci. 120 (August), 12–22. https://doi.org/10.1016/j.jafrearsci.2016.04.013.

Ghosh, S.K., Ramberg, H., 1976. Reorientation of inclusions by combination of pure shear and simple shear. Tectonophysics 34 (1–2), 1–70.

Goldstein, Arthur G., 1988. Factors affecting the kinematic interpretation of asymmetric boudinage in shear zones. J. Struct. Geol. 10 (7), 707–715.

Goscombe, Ben D., Passchier, Cees W., 2003. Asymmetric boudins as shear sense indicators—an assessment from field data. J. Struct. Geol. 25 (4), 575–589.

Gutiérrez-Aguilar, Fabián, Schaaf, Peter, Solís-Pichardo, Gabriela, Arrieta-García, Gerardo F., Hernández-Treviño, Teodoro, Linares-López, Carlos, 2021. Phase equilibrium modelling of the amphibolite facies metamorphism in the Yelapa-Chimo metamorphic complex, Mexico. Geosci. Front. 12 (1), 293–312.

Hanmer, Simon, 1986. Asymmetrical pull-aparts and foliation fish as kinematic indicators. J. Struct. Geol. 8 (2), 111–122.

Imber, J., Holdsworth, R.E., Butler, C.A., Strachan, R.A., 2001. A reappraisal of the Sibson-Scholz fault zone model: the nature of the frictional to Viscous ("Brittle-Ductile") transition along a long-lived, Crustal-scale fault, outer Hebrides, Scotland. Tectonics 20 (5), 601–624.

Jackson, N.J., Ramsay, C.R., 1980. Time-space relationships of upper precambrian Volcanic and sedimentary units in the central Arabian Shield. J. Geol. Soc. 137 (5), 617–628. https://doi.org/10.1144/gsjgs.137.5.0617.

Kretz, Ralph, 1983. Symbols for rock-Forming minerals. Am. Mineral. 68 (1–2), 277–279.

Kwékam, Maurice, Liégeois, Jean-Paul, Njonfang, Emmanuel, Pascal, Affaton, Hartmann, Gerald, Tchoua, Félix, 2010. Nature, origin and significance of the Fomopéa Pan-African high-K calc-alkaline plutonic complex in the central African Fold Belt (Cameroon). J. Afr. Earth Sci. 57 (1–2), 79–95. https://doi.org/10.1016/j.jafrearsci.2009.07.012.

Lavreau, J., Poidevin, J.L., 1990. Contribution to the geochronology of the basement of Central African Republic. J. Afr. Earth Sci. 11, 69–82.

Lavreau, J., Poidevin, J.L., Ledent, D., Liegeois, J.P., Weis, D., 1990. Contribution to the geochronology of the basement of the Central African Republic. J. Afr. Earth Sci. (and the Middle East), Heat Flow Geothermal processes 11 (1), 69–82. https://doi.org/10.1016/0899-5362(90)90078-S.

Madani, Ahmed, 2014. Assessment and evaluation of band ratios, Brovey and HSV techniques for lithologic discrimination and mapping using Landsat ETMˆ Sup+ˆ and SPOT-5 data. Int. J. Geosci. 5 (1), 5.

Mapoka, Hubert, Y., Prince Emilien, Danguene, Jean Paul, Nzenti, Jean, Biandja, Boniface, Kankeu, Emmanuel Suh, Sheo, 2011. Major structural features and the tectonic evolution of the Bossangoa- Bossembele basement, northwestern Central African Republic. Open Geol. J. 5, 21–32.

Moreau, C., M Regnoult, J.-, Déruelle, B., Robineau, B., 1987. A new tectonic model for the Cameroon line, central Africa. Tectonophysics 141 (4), 317–334. https://doi.org/10.1016/0040-1951(87)90206-X.

Neves, Brito, Bley, Benjamin, William, R., Van Schmus, Allen, Fetter, 2002. North-western Africa–north-eastern Brazil. Major tectonic links and correlation problems. J. Afr. Earth Sci. 34 (3–4), 275–278.

Ngako, V., Jégouzo, P., Nzenti, J.P., 1991. Le Cisaillement Centre Camerounais. Rôle Structural et Géodynamique Dans l'orogenèse Panafricaine. Comptes Rendus Académique Sciences Paris 313, 457–463.

Ngako, V., Affaton, P., Nnange, J.M., Njanko, Th, 2003. Pan-african tectonic evolution in central and southern Cameroon: transpression and transtension during sinistral shear movements. J. Afr. Earth Sci. 36, 207–214.

Ngako, V., Affaton, P., Njonfang, E., 2008. Pan-african tectonics in northwestern Cameroon: implication for the history of western Gondwana. Gondwana Res. 14, 509–522.

Ngnotué, T., Nzenti, J.P., Barbey, P., Tchoua, F.M., 2000. The Ntui-Betamba high-Grade gneisses: a northward extension of the Pan-African Yaoundé gneisses in Cameroon. J. Afr. Earth Sci. 31 (2), 369–381.

Njanko, Théophile, Nédélec, Anne, Pascal, Affaton, 2006. Synkinematic high-K calc-alkaline plutons associated with the Pan-African Central Cameroon shear zone (W-Tibati area): petrology and geodynamic significance. J. Afr. Earth Sci. 44 (4–5), 494–510.

Njome, M.S., Suh, C.E., 2005. Tectonic evolution of the tombel Graben basement, southwestern Cameroon. Episodes-Newsmagazine of the International Union of Geological Sciences 28 (1), 31–41.

Njonfang, Emmanuel, Vincent, Ngako, Maurice, Kwekam, Pascal, Affaton, 2006. Les orthogneiss Calco-Alcalins de Foumban–Bankim: Témoins d'une zone interne de Marge active Panafricaine En Cisaillement. Compt. Rendus Geosci. 338 (9), 606–616.

Njonfang, Emmanuel, Vincent, Ngako, Moreau, Christian, Pascal, Affaton, Diot, Hervé, 2008. Restraining bends in high temperature shear zones: the "Central Cameroon shear zone". Central Africa'. *Journal of African Earth Sciences* 52 (1–2), 9–20.

Nomo, Emmanuel Negue, Tchameni, Rigobert, Olivier, Vanderhaeghe, Sun, Fenguye, Barbey, Pierre, Tekoum, Léontine, Tchunte, Periclex Martial Fosso, Eglinger, Aurélien, Alliance Saha Fouotsa, Nicaise, 2017. Structure and LA-ICP-MS zircon U–Pb dating of syntectonic plutons emplaced in the Pan-African Banyo-Tcholliré shear zone (central north Cameroon). J. Afr. Earth Sci. 131, 251–271.

Ntieche, Benjamin, Mohan, M. Ram, Amidou, Moundi, 2017. Granitoids of the Magba shear zone, west Cameroon, central Africa: evidences for emplacement under transpressive tectonic regime. J. Geol. Soc. India 89 (1), 33–46.

Nzenti, J.P., Barbey, P., Macaudiere, J., Soba, D., 1988. Origin and evolution of the late precambrian high-grade Yaounde gneisses (Cameroon). Precambrian Res. 38 (2), 91–109. https://doi.org/10.1016/0301-9268(88)90086-1.

Njiosseu, Evine, Tanko, Laure, Nzenti, Jean-Paul, Njanko, Théophile, Kapajika, Badibanga, Nédélec, Anne, 2005. New UPb zircon ages from Tonga (Cameroon): Coexisting Eburnean–Transamazonian (2.1 Ga) and Pan-African (0.6 Ga) imprints. Compt. Rendus Geosci. 337 (6), 551–562.

Nzenti, Jean Paul, Kapajika, Badibanga, Wörner, Gerhard, Lubala, Toto Ruananza, 2006. Synkinematic emplacement of granitoids in a Pan-African shear zone in Central Cameroon. J. Afr. Earth Sci. 45 (1), 74–86.

Passchier, C.W., Trouw, R.A.J., 1998. Deformation mechanisms. In: Microtectonics, 25–56. Springer.

Passchier, C.W., Ten Brink, C.E., Bons, P.D., Sokoutis, D., 1993. δ objects as a Gauge for stress sensitivity of strain rate in Mylonites. Earth Planet Sci. Lett. 120 (3–4), 239–245.

Penaye, J., Toteu, S.F., Tchameni, R., Van Schmus, W.R., Tchakounté, J., Ganwa, A., Minyem, D., Nsifa, E.N., 2004. The 2.1Ga West Central African belt in cameroon: extension and evolution. J. Afr. Earth Sci. 39 (3), 159–164. https://doi.org/10.1016/j.jafrearsci.2004.07.053.

Pin, C., Poidevin, J.L., 1987. U-Pb zircon evidence for a Pan-African granulite facies metamorphism in the Central African Republic. A new interpretation of the high Grade series of the northern border of the Congo craton. Precambrian Res. 36, 303–312.

Poidevin, J.L., 1991. Les Ceintures de Roches Vertes de La Rrpublique Centrafricaine (Mbomou, Bandas, Boufoyo et Bogoin). Contribution h La Connaissance Du Prrcambrien Du Nord Du Craton Du Congo.' Thesis. Univ. Blaise Pascal, Clermont-Ferrand.

Poidevin, J.L., Pin, C., 1983. 1986. '2 Ga U-Pb zircon dating of Mbi Granodiorite (Central African Republic) and its bearing on the chronology of the proterozoic of central Africa. J. Afr. Earth Sci. 5 (6), 581–587.

Poidevin, J.L., Dostal, J., Dupuy, C., 1981. Archaean Greenstone belt from the Central African Republic (Equatorial Africa). Precambrian Res. 16 (3), 157–170. https://doi.org/10.1016/0301-9268(81)90011-5.

Rajendran, Sankaran, Nasir, Sobhi, 2019. ASTER capability in mapping of mineral resources of Arid region: a review on mapping of mineral resources of the Sultanate of Oman. Ore Geol. Rev. 108, 33–53.

Rajendran, Sankaran, Thirunavukkarasu, A., Balamurugan, G., Shankar, K., 2011. Discrimination of iron ore deposits of granulite terrain of southern Peninsular India using ASTER data. J. Asian Earth Sci. 41 (1), 99–106.

Rolin, P., 1992. Présence d'un chevauchement ductile Majeur d'âge Panafricain Dans La Partie centrale de La République Centrafricaine : Résultats Préliminaires. C.R. Acad. Sci. Paris 315, 467–470.

Rolin, P., 1995. La zone de Décrochements Panafricains des oubanguides En République Centrafricaine. ' *C.R.Acad. Sci. Paris* série IIa 63–69.

Sabins, F.F., 1997. Remote Sensing- Principles and Interpretation, third ed. edition, 1997. W.H. Freeman, New York, NY.

Saha-Fouotsa, Alliance Nicaise, Tchameni, Rigobert, Olivier, Vanderhaeghe, Zeh, Armin, Periclex Martial Fosso Tchunte, Eglinger, Aurélien, Emmanuel Negue Nomo, Barbey, Pierre, 2021. Lu-Hf Isotopic data of the Mbé-Sassa-Mbersi Tonalite (Central Cameroon domain): indicator of ca. 1.0 Ga Juvenile Tonian magmatism in the region. J. Geosci. Environ. Protect. 9 (9), 1–19.

Sawyer, Edward W., 2008. Atlas of Migmatites, 9. NRC Research press.

Seguem, Naïmou, Alembert Alexandre, Ganwa, Klötzli, Urs, Diguim Kepnamou, Amadou, Georges Emmanuel, Ekodeck, 2014. Petrography and geochemistry of precambrian basement straddling the Cameroon-Chad border: the Touboro Baïbokoum area. Int. J. Geosci. 5 (4), 418.

Seguem, Naïmou, Diondoh, Mbaguedjé, Diguim Kepnamou, Amadou, Mama, Ntoumbé, Sami, Mabrouk, Alembert Alexandre, Ganwa, Georges Emmanuel, Ekodeck, 2022. Petrography and geochemistry of Baïbokoum-Touboro-Ngaoundaye granitoids on the Chad-Cameroon-RCA borders (Adamawa-Yade domain). Open J. Geol. 12 (2), 136–155.

Suh, C.E., Dada, S.S., 1997. Fault rocks and differential reactivity of minerals in the Kanawa Violaine uraniferous vein, NE Nigeria. J. Struct. Geol. 19 (8), 1037–1044.

Sultan, Mohamed, Arvidson, Raymond E., Sturchio, Neil C., Guinness, Edward A., 1987. Lithologic mapping in Arid regions with Landsat thematic mapper data: Meatiq Dome, Egypt. Geol. Soc. Am. Bull. 99 (6), 748–762.

Swanson, Mark T., 1992. Late Acadian-Alleghenian transpressional deformation: evidence from asymmetric boudinage in the casco Bay area, Coastal Maine. J. Struct. Geol. 14 (3), 323–341.

Tchakounté, J., Eglinger, A., Toteu, S.F., Zeh, A., Nkoumbou, C., Mvondo-Ondoa, J., Penaye, J., De Wit, M., Barbey, P., 2017. The Adamawa-Yadé domain, a piece of archaean crust in the neoproterozoic central African orogenic belt (Bafia area, Cameroon). Precambrian Res. 299, 2010–2229.

Tchameni, R., Pouclet, A., Penaye, J., Ganwa, A.A., Toteu, S.F., 2006. Petrography and geochemistry of the Ngaoundéré Pan-African granitoids in Central North Cameroon: implications for their sources and geological setting. J. Afr. Earth Sci. 44 (4–5), 511–529. https://doi.org/10.1016/j.jafrearsci.2005.11.017.

Tchankam, Nguiessi, Clovis, Nzentui, Jean-Paul, Nkonguin Nsifa, Emmanuel, Paul, Tempier, Tchoua, Félix, 1997. Les Granitoïdes Calco-Alcalins, syn-Cisaillement de Bandja Dans La Chaîne Panafricaine Nord-Équatoriale Au Cameroun. Comptes Rendus Acad. Sci. - Ser. IIA Earth Planet. Sci. 325 (2), 95–101.

Tcheumenak Kouémo, Jules, Njanko, Théophile, Kwékam, Maurice, Naba, Séta, Bella Nké, Bertille E., Yakeu Sandjo, Angeline F., Fozing, Eric M., Njonfang, Emmanuel, 2014. Kinematic evolution of the Fodjomekwet-Fotouni Shear Zone (West-Cameroon): Implications for emplacement of the Fomopéa and Bandja plutons. J. Afr. Earth Sci. 99 (November), 261–275. Special Volume of the 24th Colloquium of African Geology.

Topak, Yusuf, Mamadou, Traore, İnan Sevimli, Ulaş, Senem, Tekin, 2022. Mineral exploration and lithological mapping using remote sensing approaches in between Yazıhan-Hekimhan (Malatya) Turkey. Bilge Int. J. Sci. Technol. Res. 6 (1), 52–61.

Topien, Rodrigue Martial, 2012. 'Pétrologie structurale et géochimique des granitoïdes de la région de Fambélé Garoua Boulaï (Ouest R.C.A.)'. Master 2. Dschang: Université de Dschang (Cameroun).

Toteu, Sadrack Félix, Penaye, Joseph, Deloule, Etienne, Van Schmus, William Randall, Tchameni, Rigobert, 2006. Diachronous evolution of volcano-sedimentary basins north of the Congo craton: Insights from U–Pb ion microprobe dating of zircons from the Poli, Lom and Yaoundé Groups (Cameroon). J. Afr. Earth Sci., The Precambrian of Central Africa 44 (4), 428–442. https://doi.org/10.1016/j.jafrearsci.2005.11.011.

Toteu, Sadrack Félix, de Wit, Maarten, Penaye, Joseph, Drost, Kerstin, Tait, Jennifer Alice, Bouyo, Merlain Houketchang, Van Schmus, William Randall, et al., 2022. Geochronology and correlations in the Central African Fold Belt along the northern edge of the Congo Craton: New insights from U-Pb dating of zircons from Cameroon, Central African Republic, and south-western Chad. Gondwana Res. 107 (July), 296–324. https://doi.org/10.1016/j.gr.2022.03.010.

Toteu, Sadrack Félix, Joseph, Penaye, Poudjom Djomani, Yvette, 2004. Geodynamic evolution of the Pan-African belt in central Africa with special reference to Cameroon. Can. J. Earth Sci. 41 (1), 73–85.

Toteu, S.F., Van Schmus, W.R., Penaye, J., Michard, A., 2001. New U–Pb and Sm–Nd data from north-Central Cameroon and its bearing on the pre-Pan African history of central Africa. Precambrian Res. 108, 45–73.

Traore, Mamadou, Çan, Tolga, Tekin, Senem, 2020. Discrimination of iron deposits using feature oriented principal component selection and band ratio methods: eastern Taurus/Turkey. Int. J. Environ. Geoinform 7, 147–156.

Traore, Mamadou, Lee, Mai Son, Rasul, Azad, Abel, Balew, 2021. Assessment of Land use/land cover changes and their impacts on Land surface temperature in Bangui (the Capital of Central African Republic). Environ. Chall. 4, 100114.

Traore, Mamadou, Can, Tolga, Tekin, Senem, 2022. Mapping carbonate-hosted Pb-Zn mineralization zones in Yahyali Province (eastern Taurus-Turkey) using ASTER data. Adv. Space Res. 69 (1), 266–281.

Vauchez, A., Neves, S., Caby, R., Corsini, M., Egydio-Silva, M., Arthaud, M., Amaro, V., 1995. The Borborema shear zone system, NE Brazil. J. South Am. Earth Sci. Geol. Borborema Province, Northeast Brazil 8 (3), 247–266. https://doi.org/10.1016/0895-9811(95)00012-5.

Xiong, Yihui, Zuo, Renguang, 2020. Recognizing multivariate geochemical anomalies for mineral exploration by combining deep learning and one-class support vector machine. Comput. Geosci. 140, 104484.